Mon. Not. R. Astron. Soc. **339,** 1057–1080 (2003)

Constraining galaxy formation and cosmology with the conditional luminosity function of galaxies

Xiaohu Yang,[1,2]★ H. J. Mo[1] and Frank C. van den Bosch[1]★

[1]*Max-Planck-Institut für Astrophysik, Karl Schwarzschild Str. 1, Postfach 1317, 85741 Garching, Germany*
[2]*Centre for Astrophysics, University of Science and Technology of China, Hefei, Anhui 230026, China*

Accepted 2002 November 5. Received 2002 November 5; in original form 2002 July 4

ABSTRACT

We use the conditional luminosity function $\Phi(L \mid M)\,\mathrm{d}L$, which gives the number of galaxies with luminosities in the range $L \pm \mathrm{d}\,L/2$ that reside in a halo of mass M, to link the distribution of galaxies to that of dark matter haloes. Starting from the number density of dark matter haloes predicted by current models of structure formation, we seek the form of $\Phi(L \mid M)$ that reproduces the galaxy luminosity function and the luminosity dependence of the galaxy clustering strength. We test the models of $\Phi(L \mid M)$ by comparing the resulting mass-to-light ratios with constraints from the Tully–Fisher (TF) relation and from galaxy clusters. A comparison between model predictions and current observations yields a number of stringent constraints on both galaxy formation and cosmology. In particular, this method can break the degeneracy between Ω_0 and the power-spectrum normalization σ_8, inherent in current weak-lensing and cluster-abundance studies. For flat ΛCDM cosmogonies with σ_8 normalized by recent weak gravitational lensing observations, the best results are obtained for $\Omega_0 \sim 0.3$; $\Omega_0 \lesssim 0.2$ leads to too large galaxy correlation lengths, while $\Omega_0 \gtrsim 0.4$ gives too high mass-to-light ratios to match the observed TF relation. The best-fitting model for the ΛCDM concordance cosmology with $\Omega_0 = 0.3$ and $\Omega_\Lambda = 0.7$ predicts mass-to-light ratios that are slightly too high to match the TF relation. We discuss a number of possible effects that might remedy this problem, such as small modifications of σ_8 and the Hubble parameter with respect to the concordance values, the assumption that the Universe is dominated by warm dark matter, systematic errors in current observational data, and the existence of dark galaxies. We use the conditional luminosity function derived from the present data to predict several statistics about the distribution of galaxy light in the local Universe. We show that roughly 50 per cent of all light is produced in haloes less massive than $2 \times 10^{12}\,h^{-1}\,\mathrm{M}_\odot$. We also derive the probability distribution $P(M \mid L)\,\mathrm{d}M$ that a galaxy of luminosity L resides in a halo with virial masses in the range $M \pm \mathrm{d}M/2$.

Key words: galaxies: clusters: general – galaxies: formation – cosmology: theory – dark matter – large-scale structure of Universe.

1 INTRODUCTION

It is well established that galaxies reside in extended dark matter haloes. Because of this, the standard assumptions in the current paradigm of structure formation are that a weakly interacting mass component (such as the cold dark matter, hereafter CDM) dominates the mass of the Universe and that galaxies form by the cooling and condensation of gas in dark matter haloes. Numerical simulations and analytical models can now give us a fairly detailed picture of the abundance and clustering of CDM haloes (e.g. Mo & White 2002). However, in order to build a coherent picture of galaxy formation, we need to be able to link these properties of the halo population to those of the galaxy population. In other words, we need to know how dark matter haloes are populated by galaxies.

Three different approaches have been used in the past to link galaxies to dark matter haloes. The first method tries to infer the properties of a halo from the properties of its galaxy population. The second method relies on *ab initio* models for the formation of galaxies, and the third method attempts to link the distributions of dark matter haloes and galaxies using a more statistical approach.

Mass estimates of individual dark matter haloes can be obtained from galaxy kinematics, from gravitational lensing, or from studying the X-ray haloes. However, each of these methods has its own

★E-mail: xhyang@ustc.edu.cn (XY); vdbosch@mpa-garching.mpg.de (FCvdB)

shortcomings: kinematics generally only probe the inner regions of dark matter haloes, results from gravitational lensing depend rather sensitively on the models adopted for the lensing systems, and X-ray measurements have to rely on the assumption that the gas is in hydrostatic equilibrium. Although significant progress has been made in each of these areas, the main limitation is that all these methods yield mass-to-light ratios for individual objects only. Because of this, various authors have attempted a more global approach by using a combination of galaxy luminosity functions and luminosity–velocity relations (such as the Tully–Fisher relation) to construct a distribution function for halo circular velocities (or masses), which in principle can be compared directly to the results from N-body simulations (i.e. Shimasaku 1993; Kauffmann, White & Guiderdoni 1993; Newman & Davis 2000; Gonzales et al. 2000; Bullock et al. 2001a; Kochanek 2001). Such analyses can be used to put constraints on the typical mass-to-light ratio for a population of galaxies, such as spiral galaxies. However, this method needs to make a rather unreliable conversion from an observed velocity measure, such as the maximum rotation velocity of a disc galaxy, to the virial velocity of the dark matter halo (see discussions in Gonzales et al. 2000; Kochanek 2001; van den Bosch 2002).

An alternative approach is to build *ab initio* models for the formation of galaxies, using either large numerical simulations (e.g. Katz, Weinberg & Hernquist 1996; Fardal et al. 2001; Pearce et al. 2000; Kay et al. 2002), (semi-) analytical models (e.g. White & Rees 1978; White & Frenk 1991; Kauffmann et al. 1993; Mo, Mao & White 1998; Somerville & Primack 1999; Cole et al. 2000; Benson et al. 2002; van den Bosch 2001, 2002), or a combination of both (Kauffmann, Nusser & Steinmetz 1997; Kauffmann et al. 1999; Diaferio et al. 1999; Benson et al. 2000, 2001; Springel et al. 2001; Mathis et al. 2002). Although these methods have yielded many useful predictions about how dark matter haloes are populated by galaxies of different intrinsic properties, many of the physical processes (such as star formation and feedback) involved are still poorly understood at the present and so some uncertain assumptions have to be made about a number of model ingredients such as the efficiency of star formation and feedback, the stellar initial mass function, and the amount of dust extinction.

With the advent of large, homogeneous data sets such as the Two Micron All Sky Survey (2MASS), the Two Degree Field Galaxy Redshift Survey (2dFGRS), and the Sloan Digital Sky Survey (SDSS), it becomes possible to address the link between dark matter haloes and galaxies using a more statistical approach. The population of galaxies in individual haloes can formally be represented by a halo-occupation function, $P(N\mid M)$, which gives the probability that a halo of mass M contains N galaxies (with certain intrinsic properties). Together with an assumption about the spatial distribution of galaxies in individual haloes, $P(N\mid M)$ is sufficient to transform the abundance and clustering of the halo population into those of the galaxy population. Numerous studies in the past have used models of $P(N\mid M)$ to study the bias and various other clustering statistics of the galaxy distribution (e.g. Jing, Mo & Börner 1998; Peacock & Smith 2000; Seljak 2000; Scoccimarro et al. 2001; White 2001; Jing, Börner & Suto 2002; Berlind & Weinberg 2002; Bullock, Wechsler & Somerville 2002; Scranton 2002; Kang et al. 2002; Marinoni & Hudson 2002). The disadvantage of this method is that it does not provide a physical understanding of the resulting halo occupation function, and as such it is complementary to the semi-analytical modelling described above.

Clearly, $P(N\mid M)$ is closely related to how galaxies form in dark matter haloes, and so is an important quantity in the theory of galaxy formation. However, $P(N\mid M)$ only contains information about the *number* of galaxies per halo (brighter than a certain lower limit). Probably the most important characteristic of a galaxy is its luminosity L. In this paper we therefore extend the halo-occupation modelling technique by labelling the galaxies with luminosities. We use the 'conditional luminosity distribution', $P(L\mid M)\,\mathrm{d}L$, which gives the probability of finding a galaxy with luminosity in the range $L\pm\mathrm{d}L/2$ as a function of halo mass M, to address the clustering and abundance of galaxies *both as function of luminosity*. In most of what follows, we focus only on the mean of this probability distribution, $\Phi(L\mid M)\,\mathrm{d}L$, which gives the average number of galaxies with luminosities in the range $L\pm\mathrm{d}L/2$ as a function of halo mass M. In what follows we refer to $\Phi(L\mid M)$ as the 'conditional luminosity function'. It is easy to see that the conditional luminosity function provides a direct link between the galaxy luminosity function (hereafter LF) $\Phi(L)\,\mathrm{d}L$, which gives the number of galaxies per comoving volume with luminosities in the range $L\pm\mathrm{d}L/2$, and the halo mass function $n(M)\,\mathrm{d}M$, which gives the number of dark matter haloes per comoving volume with masses in the range $M\pm\mathrm{d}M/2$, according to

$$\Phi(L)=\int_0^\infty \Phi(L|M)n(M)\,\mathrm{d}M. \tag{1}$$

We use this equation to place constraints on $\Phi(L\mid M)$ by using the halo mass function given by currently favoured cosmological models and the observed galaxy LF from the 2dFGRS. It is easy to see that there are an infinite number of different $\Phi(L\mid M)$ that result in exactly the same $\Phi(L)$ for given $n(M)$. We thus need additional constraints. One such constraint we use is the luminosity dependence of the galaxy–galaxy two-point correlation function $\xi_{\rm gg}(r)$ obtained from the 2dFGRS by Norberg et al. (2001). In addition, we also use $\Phi(L\mid M)\,\mathrm{d}L$ to compute the average total luminosity of galaxies in a halo of mass M,

$$\langle L\rangle(M)=\int_0^\infty \Phi(L|M)L\,\mathrm{d}L, \tag{2}$$

and compare the resulting average mass-to-light ratios as function of halo mass, $\langle M/L\rangle(M)$, with observational estimates on the scales of galaxy clusters and individual galaxies (from the Tully–Fisher relation). This allows us to break the model degeneracy and to place interesting constraints both on galaxy formation and on cosmology.

This paper is organized as follows. In Section 2 we first give an overview of the observational constraints used in this paper. Section 3 presents our model for the conditional luminosity function, and the method used to compute luminosity functions, mass-to-light ratios and correlation lengths as function of luminosity. Results for the ΛCDM concordance model are presented in Section 4. In Section 5 we discuss possible systematic errors in current observational data that may affect our results. Section 6 presents models for different cosmologies and for different assumptions about the nature of the dark matter. A detailed comparison with results obtained from semi-analytical models for the formation of galaxies is presented in Section 7. In Section 8 we use the conditional LF to present several statistics regarding the distribution of light in the local Universe, and we summarize our results in Section 9.

Throughout this paper we define M to be the halo mass inside the radius $R_{\rm vir}$ inside of which the average density is 180 times the cosmic mean density. All luminosities are in the photometric b_j band and we convert all units to $h=1$, where $h=H_0/(100\,\mathrm{km\,s^{-1}})$.

2 OBSERVATIONAL CONSTRAINTS

2.1 The galaxy luminosity function

Galaxy LFs are typically obtained from large redshift surveys, the size and accuracy of which have improved steadily over the years. (e.g. Efstathiou, Ellis & Peterson 1988a; Loveday et al. 1992; Marzke, Huchra & Geller 1994; Zucca et al. 1997; Folkes et al. 1999). The most recent determinations of the LF of 'field' galaxies are those from the Las Campanas Redshift Survey (LCRS; Lin et al. 1996), the SDSS commissioning data (Blanton et al. 2001) and the 2dFGRS (Norberg et al. 2002). In this paper we use the LF of the 2dFGRS, which is currently the largest published redshift survey, including more than 110 500 galaxies with $17.0 < b_j < 19.2$ and $z < 0.25$. After applying k corrections, correcting the magnitudes for galaxy evolution and zero-point offsets, and correcting the measured number densities for incompleteness, Norberg et al. derive a b_j LF spanning the magnitude range $-22.5 \lesssim M_{b_j} - 5\log h \lesssim -14.0$ which is well fitted by a Schechter (1976) function

$$\Phi(L)\mathrm{d}L = \frac{\Phi^*}{L^*}\left(\frac{L}{L^*}\right)^{\alpha} \exp(-L/L^*)\,\mathrm{d}L, \tag{3}$$

with $L^* = 9.64 \times 10^9\, h^{-2}\,\mathrm{L}_\odot$ (where we have used $\mathrm{M}_{\odot,b_j} = 5.3$), $\alpha = -1.21$ and $\Phi^* = 1.61 \times 10^{-2}\, h^3\,\mathrm{Mpc}^{-3}$. The derivation of a luminosity function is cosmology-dependent, and the parameters listed above correspond to $\Omega_0 = 0.3$ and $\Omega_\Lambda = 0.7$.[1]

2.2 The galaxy correlation function

Numerous observational studies in the past have investigated differential galaxy clustering as function of luminosity. Although several of these have claimed a dependence of clustering strength on luminosity (e.g. Börner, Mo & Zhou 1989; Park et al. 1994; Benoist et al. 1996; Willmer, DaCosta & Pellegrini 1998; Guzzo et al. 2000), others found results that indicated no significant luminosity dependence (e.g. Loveday et al. 1995; Szapudi et al. 2000; Hawkins et al. 2001). The main reason for this disagreement is the relatively small size of the redshift surveys used. Recently, Norberg et al. (2001) investigated the luminosity dependence of galaxy clustering using the 2dFGRS, which is the largest extant redshift survey. After correcting their luminosities for band-shifting (k correction) and galaxy evolution they computed the two-point correlation function $\xi_{\rm gg}(r)$ for various bins in absolute magnitude. Each of these correlation functions is well fitted by a simple power law $\xi_{\rm gg}(r) = (r_0/r)^\gamma$. Although the shape of the correlation function varies little with luminosity (i.e. $\gamma \simeq 1.7 \pm 0.1$ for all bins), Norberg et al. find a clear increase of the correlation length r_0 with increasing luminosity. The correlation length $r_0(L)$ changes slowly for $L \lesssim L^*$, but increases by about a factor two from $L = L^*$ to $\simeq 5\ L^*$.

Note that the conversion of redshift into comoving distance is cosmology-dependent. The $r_0(L)$ and $\xi_{\rm gg}(r)$ that we use here, and which we adopt from Norberg et al. (2001), are computed assuming $\Omega_0 = 0.3$ and $\Omega_\Lambda = 0.7$. Note also that, although the galaxy luminosities have been corrected for evolution, the correlation function itself may also evolve with redshift, an effect that has not been corrected for. As we show below, for the redshift range covered by the 2dFGRS, this effect is not negligible.

[1] We also use LFs derived for other cosmological models, which were kindly made available to us by Shaun Cole and Peder Norberg (private communications).

2.3 Tully–Fisher relation

The Tully–Fisher (TF) relation for spiral galaxies relates a luminosity measure to a dynamical mass measure and therefore provides an observational constraint on the mass-to-light ratio for this class of galaxies. The TF relation can be written as

$$\log(L) = a_{\rm TF} + b_{\rm TF} \log V_{\rm max} \tag{4}$$

where $V_{\rm max}$ corresponds to the maximum of the observed rotation curve and $a_{\rm TF}$ and $b_{\rm TF}$ are two constants. This can be recast in an expression relating the total mass-to-light ratio to the total mass:

$$\log\left(\frac{M}{L}\right) = \left(1 - \frac{b_{\rm TF}}{3}\right)\log(M) + (1.797 b_{\rm TF} - a_{\rm TF}) - b_{\rm TF}\log\left(\frac{V_{\rm max}}{V_{\rm vir}}\right) - \frac{b_{\rm TF}}{6}\log\Omega_0. \tag{5}$$

The third term on the right-hand side of equation (5) relates the observed rotation measure to the virial velocity $V_{\rm vir}$ of the dark matter halo. Here $V_{\rm vir}$ is the circular velocity at the virial radius within which the average overdensity is 180.

We use the data obtained and collected by Tully & Pierce (2000, hereafter TP00). These authors list photometry and H I linewidths for 24 nearby galaxies for which distances are available from Cepheids (the 'local calibrator' sample), as well as similar data for a large number of galaxies in various clusters (the 'cluster' sample). Distances to these clusters are obtained by assuming that the TF relation is a universal relation. For a sample of in total 115 galaxies TP00 list the absolute B-band magnitudes and the H I linewidths. Note that these magnitudes have been corrected for inclination- and linewidth-dependent internal dust extinction. Since the luminosities used in the LF function and correlation lengths described above have *not* been corrected for internal extinction, we should also use a TF relation that has *not* been corrected for the internal dust obscuration. To do this, we use the total apparent B-band magnitudes and distance moduli listed in TP00 and compute the absolute B-band magnitudes corrected for galactic foreground extinction (based on the 100-μm cirrus maps of Schlegel, Finkbeiner & Davis 1998). These are converted to b_j-band magnitudes using $b_j = B - 0.28\,(B - V)$ (Blair & Gilmore 1982) and adopting $B - V = 0.7$, which corresponds roughly to the average colour of disc galaxies (de Jong 1996). Finally we introduce the scaling with H_0 adopting $h = 0.7$, which corresponds to the value of the Hubble constant used throughout this paper.

The resulting b_j-band TF relation is shown in the left panel of Fig. 1, where we have made the assumption that the H I linewidth is equal to twice the maximum circular velocity, $V_{\rm max}$. Using a double regression with errors in both magnitude and $V_{\rm max}$, we obtain the best-fitting TF relation $M_{b_j} - 5\log h = -4.17 - 6.67\log V_{\rm max}$, for which $a_{\rm TF} = 3.79$ and $b_{\rm TF} = 2.67$. These are the values we substitute in equation (5) to constrain the mass-to-light ratios of our models.

For a dark matter halo with a NFW density distribution (Navarro, Frenk & White 1997) the circular velocity increases from the centre, reaches a maximum $V_{\rm max}$ at $r \simeq 2.163\, r_{\rm s}$ (where $r_{\rm s}$ is the scale radius in the NFW profile) and then decreases again to reach $V_{\rm vir}$ at the virial radius $R_{\rm vir} = c r_{\rm s}$. One finds that

$$\frac{V_{\rm max}}{V_{\rm vir}} \simeq 0.465\sqrt{\frac{c(1+c)}{(1+c)\ln(1+c) - c}}. \tag{6}$$

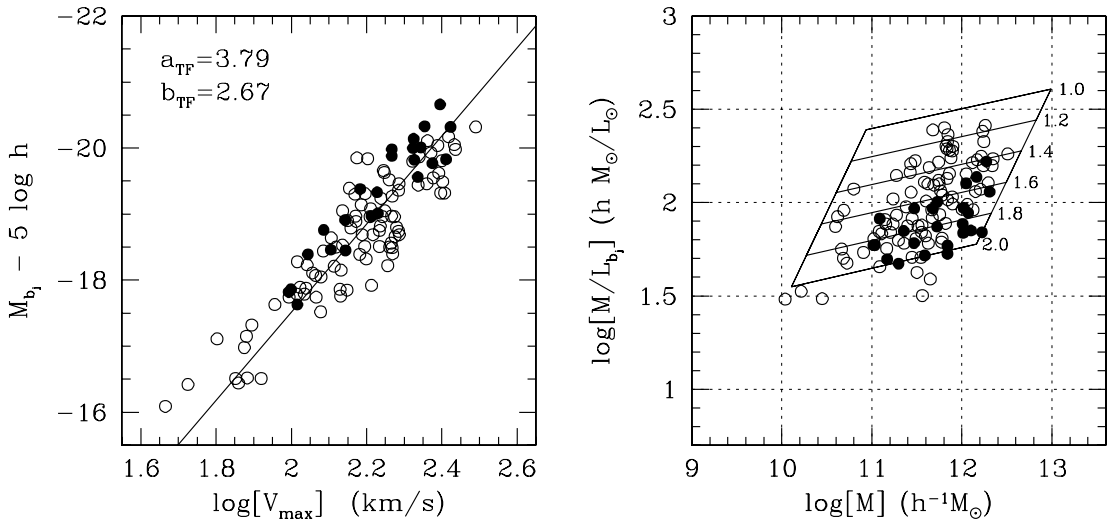

Figure 1. The left panel plots the b_j-band Tully–Fisher (TF) relation for the 'local calibrator sample' (solid circles) and the 'cluster sample' (open circles) uncorrected for intrinsic extinction (data taken from Tully & Pierce 2000). The solid line indicates the best-fitting linear regression $\log L_{b_j} = 3.79 + 2.67 \log V_{\rm max}$. The panel on the right plots the resulting mass-to-light ratios as function of halo mass, where we have adopted $V_{\rm max}/V_{\rm vir} = 1.6$. In addition, the parallelogram indicates the average mass-to-light ratios of disc galaxies obtained from the TF relation for six different values of $V_{\rm max}/V_{\rm vir}$ as indicated. See text for a more detailed discussion.

With our definition of the virial radius (see Section 1), typical galaxy sized haloes have $10 \lesssim c \lesssim 50$ (Jing 2000; Bullock et al. 2001b), corresponding to $1.2 \lesssim V_{\rm max}/V_{\rm vir} \lesssim 1.9$.[2] The maximum rotation velocity of a disc in a halo is typically larger than the $V_{\rm max}$ of the dark matter halo, because of the contribution of the baryons to the total circular velocity and the contraction of the dark matter halo during the formation of the disc (see e.g. Barnes & White 1984; Blumenthal et al. 1986; Flores et al. 1993; Mo et al. 1998; Mo & Mao 2000; van den Bosch 2002).

In the right panel of Fig. 1, we plot the mass-to-light ratios for the individual galaxies of the TP00 data set (open and solid circles) computed using $V_{\rm max}/V_{\rm vir} = 1.6$. In addition, we plot the relations between M/L and M obtained from the best-fitting linear TF relation for six different values of $V_{\rm max}/V_{\rm vir}$ as indicated. We only plot these relations over the range of masses that correspond to the magnitude range over which the TF relation of TP00 has been derived. In what follows we use these TF constraints to judge the credibility of our models, keeping in mind that for typical CDM cosmogonies one expects $1.4 \lesssim V_{\rm max}/V_{\rm vir} \lesssim 2.0$ (taking the 'boosting' effect of the baryons into account).

3 POPULATING DARK HALOES WITH GALAXIES

3.1 The dark matter mass function

The mass function of dark matter haloes at $z = 0$ can be written in the form

$$n(M)\,{\rm d}M = \frac{\bar{\rho}}{M^2}\nu f(\nu)\left|\frac{{\rm d}\ln\sigma}{{\rm d}\ln M}\right|{\rm d}M, \tag{7}$$

where $\bar{\rho}$ is the mean matter density of the Universe at $z = 0$, $\nu = \delta_{\rm c}/\sigma(M)$, $\delta_{\rm c}$ is the critical overdensity required for collapse at $z = 0$, and $f(\nu)$ is a function of ν to be specified below. The quantity $\sigma(M)$ in the above equation is the linear rms mass fluctuation on mass scale M, which is given by the linear power spectrum of density perturbations $P(k)$ as

$$\sigma^2(M) = \frac{1}{2\pi^2}\int_0^\infty P(k)\hat{W}_M^2(k)k^2\,{\rm d}k, \tag{8}$$

where $\hat{W}_M(k)$ is the Fourier transform of the smoothing filter on mass scale M.

According to the Press–Schechter formalism (Press & Schechter 1974), the function $f(\nu)$ has the universal form,

$$\nu f(\nu) = 2\left(\frac{\nu^2}{2\pi}\right)^{1/2}\exp\left(-\frac{\nu^2}{2}\right), \tag{9}$$

independent of cosmology, redshift, power spectrum and its normalization (e.g. Bond et al. 1991; Lacey & Cole 1993). However, various studies have shown that the halo mass function with this $f(\nu)$ is inconsistent with numerical simulations (e.g. Efstathiou et al. 1988a; Jain & Bertschinger 1994; Tormen 1998; Gross et al. 1998; Governato et al. 1999; Jenkins et al. 2001). Using ellipsoidal rather than spherical collapse conditions, Sheth, Mo & Tormen (2001) derived an improved form for $f(\nu)$ given by

$$\nu f(\nu) = 2A\left(1 + \frac{1}{\nu'^{2q}}\right)\left(\frac{\nu'^2}{2\pi}\right)^{1/2}\exp\left(-\frac{\nu'^2}{2}\right) \tag{10}$$

with $\nu' = \sqrt{a}\nu$, $a = 0.707$, $q = 0.3$ and $A \approx 0.322$. The resulting mass function has been shown to be in excellent agreement with numerical simulations, as long as halo masses are defined as the masses inside a sphere with an average overdensity of about 180 (Sheth & Tormen 1999; Jenkins et al. 2001). Therefore, in what follows we consistently use that definition of halo mass, and we adopt a mass function with $f(\nu)$ given by equation (10). In addition we use the CDM power spectrum of Bardeen et al. (1986), and we

[2] Note that the c used here is not the same as that in Navarro et al. (1997), Jing (2000) or Bullock et al. (2001b), because of our different definition of $R_{\rm vir}$. When computing the range of expected c we use the results of Bullock et al. (2001b) properly scaled to our definition of the virial radius.

adopt a spatial top-hat filter for which

$$\hat{W}_M(k;R) = \frac{3}{(kR)^3}[\sin(kR) - kR\cos(kR)] \tag{11}$$

where the mass M and filter radius R are related according to $M = 4\pi\bar{\rho}R^3/3$.

3.2 The conditional luminosity function

In order to compute a LF from the halo mass function, we need to specify the conditional luminosity function $\Phi(L\,|\,M)\,\mathrm{d}L$ (see equation 1), which gives the expected number of galaxies with luminosities in the range $L \pm \mathrm{d}L/2$ (in some chosen photometric band) in a halo of mass M. Note that $\Phi(L\,|\,M)$ is a statistical function, and should not be interpreted as the LF of galaxies residing in any *individual* dark matter halo.

For massive haloes, such as clusters of galaxies, that contain many galaxies the shape of $\Phi(L\,|\,M)$ should be the same as that of the cluster LF, which can be well described by a Schechter function. For all mass haloes, the average of $\Phi(L\,|\,M)$ over the halo mass function should give the field galaxy LF. Therefore, we assume that $\Phi(L\,|\,M)\,\mathrm{d}L$ can be described by a Schechter function:

$$\Phi(L|M)\mathrm{d}L = \frac{\tilde{\Phi}^*}{\tilde{L}^*}\left(\frac{L}{\tilde{L}^*}\right)^{\tilde{\alpha}} \exp(-L/\tilde{L}^*)\,\mathrm{d}L. \tag{12}$$

Here $\tilde{L}^* = \tilde{L}^*(M), \tilde{\alpha} = \tilde{\alpha}(M)$ and $\tilde{\Phi}^* = \tilde{\Phi}^*(M)$; i.e. the three parameters that describe the conditional LF depend on M. In what follows we do not explicitly write this mass dependence, but consider it understood that quantities with a tilde are functions of M.

With $\Phi(L\,|\,M)$ defined by equation (12), the total average luminosity in a halo of mass M is

$$\langle L\rangle(M) = \int_0^\infty \Phi(L\,|\,M)L\,\mathrm{d}L = \tilde{\Phi}^*\tilde{L}^*\Gamma(\tilde{\alpha}+2) \tag{13}$$

with $\Gamma(x)$ the Gamma function. The average number of galaxies brighter than $\tilde{L}^*$ in a halo of mass M is

$$\mathcal{N}^*(M) \equiv \int_{\tilde{L}^*}^\infty \Phi(L\,|\,M)\,\mathrm{d}L = \tilde{\Phi}^*\Gamma(\tilde{\alpha}+1,1). \tag{14}$$

with $\Gamma(a,x)$ the incomplete Gamma function.

For each halo, we define a 'central' galaxy, the luminosity of which we denote by L_c. We assume the central galaxy to be the brightest one in a halo, consistent with the fact that in most (if not all) haloes the brightest members reside near the centre. The mean luminosity of this central galaxy is defined as

$$\bar{L}_\mathrm{c}(M) = \int_{L_1}^\infty \Phi(L\,|\,M)L\,\mathrm{d}L = \tilde{\Phi}^*\tilde{L}^*\Gamma\left(\tilde{\alpha}+2, L_1\big/\tilde{L}^*\right), \tag{15}$$

with L_1 defined so that a halo of mass M has on average one galaxy with $L > L_1$, i.e.

$$\int_{L_1}^\infty \Phi(L\,|\,M)\,\mathrm{dL} = 1. \tag{16}$$

In most of our discussion, the luminosity of the central galaxy of a halo is assumed to be a random variable with distribution function $\Phi(L\,|\,M)$ at $L > L_1$. Motivated by numerical simulations and semi-analytical models of galaxy formation, which suggest that the luminosities of central galaxies are tightly correlated with the masses of their host haloes (e.g. Katz et al. 1996; Fardal et al. 2001; Pearce et al. 2000; Kay et al. 2002; Kauffmann et al. 1993; Somerville & Primack 1999; Cole et al. 2000), we also consider an alternative sampling in which L_c follows a log-normal distribution with mean $\bar{L}_\mathrm{c}$, and with some given width, i.e. we modify the form of $\Phi(L\,|\,M)$ by replacing the part with $L > L_1$ by a log-normal distribution. As we will show, both these two samplings of L_c give similar results.

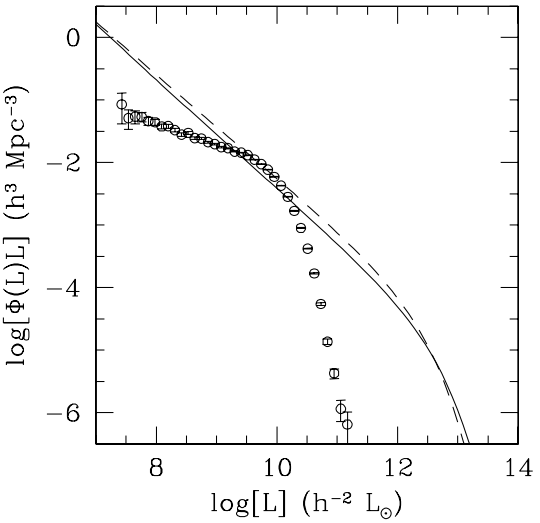

Figure 2. A comparison of the galaxy LF with the halo mass function. Open circles with error bars correspond to the 2dFGRS LF in the b_j-band. Solid (dashed) lines correspond to the LF that one would obtain from the Sheth & Tormen (Press–Schechter) halo mass function under the assumption that each halo yields exactly one galaxy with $M/L = 100\,h\,\mathrm{M}/\mathrm{L}_\odot$. Note that under such naive assumptions one expects too many both faint and bright galaxies, suggesting that in reality the M/L decreases (increases) with mass at the low (high) mass end.

In order to specify the conditional LF fully, we need to specify the mass dependence of $\tilde{\Phi}^*$, $\tilde{L}^*$ and $\tilde{\alpha}$. We are guided by a direct comparison of the halo mass function $n(M)$ and the galaxy LF, $\Phi(L)$. Under the assumption that each dark matter halo harbours exactly one galaxy, and that each system has exactly the same mass-to-light ratio M/L, the galaxy LF follows directly from the halo mass function. Fig. 2 compares the LF thus obtained assuming $M/L = 100\,h\,\mathrm{M}/\mathrm{L}_\odot$ with that of the 2dFGRS. The actual LF is steeper (shallower) than the one obtained directly from the halo mass function at high (low) luminosities. This immediately suggests that in reality, rather than being constant, $\langle M/L\rangle$ decreases with increasing mass, reaches a minimum at around L^*, and then increases again. Note that this is qualitatively consistent with simple predictions from galaxy formation models; at low mass, feedback effects cause M/L to increase, while inefficient cooling suppresses the formation of galaxies in more massive haloes. The above comparison, however, is not to be taken too seriously, since in reality not every halo harbours exactly one galaxy; some halos may be empty while others contain thousands of galaxies. The comparison in Fig. 2, and the particular value of $M/L = 100\,h\,\mathrm{M}/\mathrm{L}_\odot$, therefore only serves an illustrative purpose. Nevertheless, based on the above comparison we adopt the following parametrization for the average mass-to-light ratios:

$$\left\langle\frac{M}{L}\right\rangle(M) = \frac{1}{2}\left(\frac{M}{L}\right)_0\left[\left(\frac{M}{M_1}\right)^{-\beta} + \left(\frac{M}{M_1}\right)^{\gamma_1}\right], \tag{17}$$

which has four free parameters: a characteristic mass M_1, for which the mass-to-light ratio is equal to $(M/L)_0$, and two slopes, β and γ_1, which specify the behaviour of $\langle M/L\rangle$ at the low- and high-mass ends, respectively. For $M \ll M_1$ one has that $\langle M/L\rangle \propto M^{-\beta}$, while for $M \gg M_1$ the mass-to-light ratio increases with mass according

to $\langle M/L\rangle \propto M^{\gamma_1}$ (both β and γ_1 are assumed to, but not restricted to, be positive).

In addition we introduce a fifth free parameter, $M_{\rm min}$, which sets the mass-scale below which no galaxies form; i.e. we set $\langle L\rangle(M) = 0$ for $M < M_{\rm min}$. This additional free parameter has a physical motivation (see below), and is included to take account of the fact that the 2dFGRS LF has a faint magnitude cut-off at $M_{b_j} - 5\log h = -14.0$.

It is obvious that for galaxy-sized haloes $\tilde{L}^*$ must decrease with decreasing mass, since galaxies with $L = 10^{10}\,h^{-2}\,{\rm L}_\odot$ should not be found in a halo of $M = 10^9\,h^{-1}\,{\rm M}_\odot$. Furthermore, since the LF of the total galaxy population has an exponential tail at $L > L^*$, it is unlikely that $\tilde{L}^*$ keeps increasing with M, because otherwise we would observe galaxies brighter than, say, $100L^*$. Therefore we adopt the following parametrization for $\tilde{L}^*(M)$:

$$\frac{M}{\tilde{L}^*(M)} = \frac{1}{2}\left(\frac{M}{L}\right)_0 f(\tilde{\alpha})\left[\left(\frac{M}{M_1}\right)^{-\beta} + \left(\frac{M}{M_2}\right)^{\gamma_2}\right], \tag{18}$$

with

$$f(\tilde{\alpha}) = \frac{\Gamma(\tilde{\alpha}+2)}{\Gamma(\tilde{\alpha}+1,1)}. \tag{19}$$

This parametrization of $\tilde{L}^*(M)$ has two additional free parameters: a characteristic mass M_2 and a power-law slope γ_2. The factor $f(\tilde{\alpha})$ is to ensure that $\mathcal{N}^*(M) = 1$ for $M \ll \min[M_1, M_2]$, which is motivated by the fact that for small-mass haloes (i.e. smaller than a typical galaxy group) one expects on average only one dominant galaxy per halo. For $M \gg \max[M_1, M_2]$ this parametrization yields $\mathcal{N}^* \propto M^{\gamma_2-\gamma_1}$.

Finally, for $\tilde{\alpha}(M)$ we adopt a simple linear scaling with $\log(M)$, which we parametrize as follows:

$$\tilde{\alpha}(M) = \alpha_{15} + \eta\log(M_{15}). \tag{20}$$

Here M_{15} is the halo mass in units of $10^{15}\,h^{-1}\,{\rm M}_\odot$, $\alpha_{15} = \tilde{\alpha}(M_{15} = 1)$, and η describes the change of the faint-end slope $\tilde{\alpha}$ with halo mass. Note that once $\tilde{\alpha}(M)$ and $\tilde{L}^*(M)$ are given, the normalization of the conditional LF, $\tilde{\Phi}^*(M)$ can be specified through the mass-to-light ratio using equations (17) and (13).

Our model for $\Phi(L\,|\,M)$ specified above thus has nine free parameters: $(M/L)_0$, $M_{\rm min}$, M_1, M_2, β, γ_1, γ_2, η and α_{15}. Clearly, it is infeasible to explore the entire nine-dimensional parameter space. However, we can use observational constraints and theoretical considerations to significantly reduce the freedom of the model. First of all, we use constraints obtained from studies of the LFs of clusters of galaxies. Beijersbergen et al. (2002) derived the *B*-band LF of the Coma cluster, which is well-fitted by a Schechter function with $L^*_{\rm coma} = 6.73\times10^9\,h^{-2}\,{\rm L}_\odot$ and $\alpha_{\rm coma} = -1.32$. Therefore, we set $\alpha_{15} = -1.32$, which reduces the number of free parameters by one. Secondly, $L^*_{\rm coma}$ is very similar to L^* of the *entire* galaxy population (see Section 2). In addition, the luminosity functions of galaxies in groups and poor clusters also have characteristic luminosities similar to L^* (e.g. Muriel, Valotto & Lambas 1998). This suggests that $\tilde{L}^*$ does not increase much with mass over the range 10^{13}–$10^{15}h^{-1}{\rm M}_\odot$, and we therefore tune the value of M_2 so that $\tilde{L}^*(M_L) = L^*$ with $M_L = 10^{13.5}h^{-1}{\rm M}_\odot$. Based on a variety of observations, Fukugita, Hogan & Peebles (1998) find that clusters of galaxies, which they define as systems with $M > 10^{14}h^{-1}{\rm M}_\odot$, have a mass-to-light ratio $(M/L)_B = 450\pm100\,h\,{\rm M/L}_\odot$. Therefore, we set $\langle M/L\rangle(M) = 500\,h\,{\rm M/L}_\odot$ for $M \geqslant 10^{14}h^{-1}{\rm M}_\odot$, and tune γ_1 so that $\langle M/L\rangle\,(M)$ reaches this upper limit at $M = 10^{14}\,h^{-1}\,{\rm M}_\odot$. Finally we adopt $M_{\rm min} = 1.0\times10^9\,h^{-1}\,{\rm M}_\odot$, which corresponds roughly to the mass scale below which no galaxies can form in a reionized medium, i.e. the virial temperature is $T_{\rm vir} \lesssim 10^4$ K for such systems at the present time.

All in all we have thus reduced the number of free parameters to five: $(M/L)_0$, M_1, β, γ_2, and η. In Section 4.2 we address the impact that this reduction of the model freedom has on our results.

3.3 The galaxy correlation function

If the initial density distribution of matter is described by a Gaussian random field, the clustering properties of dark matter haloes are fully determined by the linear power spectrum $P(k)$ and cosmology (Kaiser 1984; Bardeen et al. 1986; Cole & Kaiser 1989; Mo & White 1996; Mo, Jing & White 1997; Sheth et al. 2001). Once a model is adopted for the galaxy occupation numbers of dark matter haloes (i.e. once $P(N\,|\,M)$ is specified), the clustering properties of galaxies, such as the two-point correlation function $\xi_{\rm gg}(r)$, can be computed. With our model for the conditional luminosity function $\Phi(L\,|\,M)$ described above, we basically have completely specified the differential halo occupation numbers as function of luminosity and halo mass. Therefore, once we adopt an additional model for the spatial distribution of galaxies in individual haloes, we can compute the correlation function of galaxies *as function of luminosity*. Using the definition that $\xi_{\rm gg}\,(r_0) = 1$ we compute $r_0(L)$, which we compare to the observed relation of the 2dFGRS (see Section 2.2).

We proceed as follows. We decompose the two-point galaxy–galaxy correlation function into two parts:

$$\xi_{\rm gg}(r) = \xi^{\rm 1h}_{\rm gg}(r) + \xi^{\rm 2h}_{\rm gg}(r). \tag{21}$$

Here $\xi^{\rm 1h}_{\rm gg}$ represents the correlation due to pairs of galaxies within the same halo (the '1-halo' term), while $\xi^{\rm 2h}_{\rm gg}$ describes the correlation due to galaxies that occupy different haloes (the '2-halo' term). For the 1-halo term we need to specify the distribution of galaxies in individual haloes, while the 2-halo term is given by the correlation of the population of dark matter haloes.

3.3.1 The 2-halo term

Consider all galaxies with luminosities in the range $[L_1, L_2]$, and define $\hat{\xi}_{\rm gg}(r)$ as the two-point correlation function of this subset of galaxies. By definition, the total number of pairs of galaxies *per comoving volume* in this luminosity range that have separations in the range $r \pm {\rm d}r/2$ is

$$n_{\rm pair} = \frac{\bar{n}^2_{\rm g}}{2}[1 + \hat{\xi}_{\rm gg}(r)]4\pi r^2\,{\rm d}r. \tag{22}$$

where the factor $1/2$ corrects for double counting of each pair. Here $\overline{n}_{\rm g}$ is the mean number density of galaxies with $L \in [L_1, L_2]$ which is given by

$$\bar{n}_{\rm g} = \int_0^\infty n(M)\langle N(M)\rangle\,{\rm d}M, \tag{23}$$

and

$$\langle N(M)\rangle = \int_{L_1}^{L_2}\Phi(L|M)\,{\rm d}L \tag{24}$$

gives the mean number of galaxies in the specified luminosity range for haloes of mass M.

Consider a galaxy with $L \in [L_1, L_2]$ that lives in a halo of mass M_1. There are, on average, $n(M_2)\,4\pi r^2\,{\rm d}r$ dark matter haloes with mass M_2 that are separated from this galaxy by a distance in the range $r \pm {\rm d}r/2$. In each of these haloes there are on average $\langle N(M_2)\rangle$ galaxies that also have a luminosity in the range $[L_1, L_2]$. Integrating

over the halo mass function, and taking account of the clustering properties of dark matter haloes, we obtain the *excess* number N_+ of galaxy pairs *per galaxy in a halo of mass* M_1 with separations in the range $r \pm \mathrm{d}r/2$:

$$N_+(M_1) = 4\pi r^2\,\mathrm{d}r \int_0^\infty n(M_2)\langle N(M_2)\rangle \xi_{\rm hh}(r; M_1, M_2)\,\mathrm{d}M_2. \tag{25}$$

Here $\xi_{\rm hh}(r; M_1, M_2)$ is the cross-correlation between dark matter haloes of mass M_1 and M_2. Note that we implicitly assume that all galaxies in a given halo are located at the halo centre. Since the separation between individual haloes is typically much larger than the separation between galaxies in the same halo, this simplification does not influence our results for large r.

Multiplying $N_+(M_1)$ with $\langle N(M_1)\rangle$ and integrating over the halo mass function gives the total excess number of galaxy pairs *per comoving volume* with separations in the required range. Combining this with equation (22) yields

$$\frac{\bar{n}_{\rm g}^2}{2}\hat{\xi}_{\rm gg}^{\rm 2h}(r)4\pi r^2\mathrm{d}r = \frac{1}{2}\int_0^\infty \mathrm{n(M_1)\langle N(M_1)\rangle N_+(M_1)\,dM_1}. \tag{26}$$

What remains is to specify the dark halo correlation function $\xi_{\rm hh}(r; M_1, M_2)$. Mo & White (1996) developed a model, based on the Press–Schechter formalism, that describes the bias of dark matter haloes of mass M with respect to the dark matter mass distribution. This model was extended by Sheth et al. (2001) to account for ellipsoidal collapse. According to this,

$$\xi_{\rm hh}(r; M_1, M_2) = b(M_1)b(M_2)\xi_{\rm dm}^{\rm 2h}(r), \tag{27}$$

where $\xi_{\rm dm}^{\rm 2h}(r)$ is the 2-halo term of the dark matter mass correlation function (see below) and

$$b(M) = 1 + \frac{1}{\sqrt{a}\delta_{\rm sc}(z)}\left[\sqrt{a}(a\nu^2) + \sqrt{a}b(a\nu^2)^{1-c} - \frac{(a\nu^2)^c}{(a\nu^2)^c + b(1-c)(1-c/2)}\right], \tag{28}$$

with $a = 0.707, b = 0.5, c = 0.6$ and $\nu = \delta_{\rm c}/\sigma(M)$ (Sheth et al. 2001). This model has been shown to match accurately the correlation function of dark matter haloes in N-body simulations (Jing 1998; Sheth & Tormen 1999).

Substituting equations (27) and (25) in (26) we obtain

$$\hat{\xi}_{\rm gg}^{\rm 2h}(r) = \bar{b}^2\xi_{\rm dm}^{\rm 2h}(r), \tag{29}$$

where

$$\bar{b} = \frac{1}{\bar{n}_{\rm g}}\int_0^\infty n(M)\langle N(M)\rangle b(M)\,\mathrm{d}M. \tag{30}$$

Note that the dark matter mass correlation function in the above expression is the 2-halo term (i.e. the 1-halo term is irrelevant for the halo–halo correlation). Using the same concept as in equation (21) we can write that $\xi_{\rm dm}^{\rm 2h}(r) = \xi_{\rm dm}(r) - \xi_{\rm dm}^{\rm 1h}r)$. Here $\xi_{\rm dm}(r)$ is the non-linear two-point correlation function of the dark matter distribution, and $\xi_{\rm dm}{}^{\rm 1h}(r)$ is the 1-halo term. The Fourier transform of the one-halo term is given by

$$P_{\rm dm}^{\rm 1h}(k) = \int_0^\infty n(M)[\hat{\delta}(M;k)]^2\,\mathrm{d}M, \tag{31}$$

where

$$\hat{\delta}(M;k) = \int_0^\infty \frac{\rho(r)}{\bar{\rho}}\mathrm{e}^{-\mathrm{i}\boldsymbol{k}\cdot\boldsymbol{r}}\,\mathrm{d}^3\boldsymbol{r} \tag{32}$$

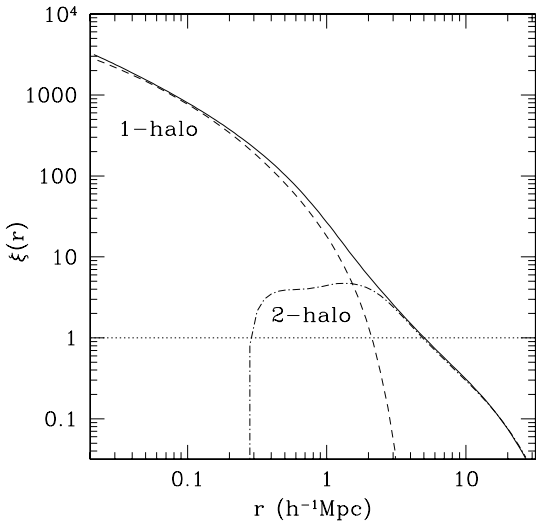

Figure 3. The non-linear dark matter mass correlation function $\xi_{\rm dm}(r)$ of the ΛCDM 'concordance' model (solid line). The dashed and dot–dashed lines indicate the '1-halo' and '2-halo' terms, respectively. Note that the correlation length r_0, defined as $\xi_{\rm dm}(r_0) = 1$ (dotted line), is determined by the '2-halo' term only.

is the Fourier transform of the halo density profile $\rho(r)$ (e.g. Neyman & Scott 1952; McClelland & Silk 1977; Ma & Fry 2000). We assume that $\rho(r)$ has the NFW form

$$\rho(r) = \frac{\bar{\delta}\bar{\rho}}{(r/r_{\rm s})(1 + r/r_{\rm s})^2}, \tag{33}$$

where $r_{\rm s}$ is a characteristic radius, $\bar{\rho}$ is the average density of the Universe, and $\bar{\delta}$ is a dimensionless amplitude which can be expressed in terms of the halo concentration parameter $c = R_{\rm vir}/r_{\rm s}$ as

$$\bar{\delta} = \frac{180}{3}\frac{c^3}{\ln(1+c) - c/(1+c)}. \tag{34}$$

Numerical simulations show that c is correlated with halo mass, and we use the relation given by Bullock et al. (2001b), converted to the c appropriate for our definition of $R_{\rm vir}$.

The 1-halo and 2-halo terms of the dark matter two-point correlation function thus obtained are shown in Fig. 3 for a ΛCDM model with $\Omega_0 = 0.3$, $\Omega_\Lambda = 0.7$, $h = 0.7$ and $\sigma_8 = 0.9$. Here we have used the fitting formula for $\xi_{\rm dm}(r)$ given by Peacock & Dodds (1996). Note that for $r \gtrsim 3\,h^{-1}$ Mpc, $\xi_{\rm dm}(r)$ is dominated by the 2-halo term, while for $r \lesssim 1\,h^{-1}$ Mpc the 1-halo term dominates. Therefore as long as $\bar{b}$ is sufficiently large, r_0 is determined by the 2-halo term only. In this case, the value of r_0 depends only on the mean occupation number $\langle N(M)\rangle$ and is independent of the details of how galaxies are distributed in individual haloes. In practice, we always find that at $r = r_0$ the 2-halo term dominates, and we therefore use equation (29) to compute the galaxy–galaxy correlation function for galaxies with $L \in [L_1, L_2]$ from which we obtain $r_0(L)$ by solving $\hat{\xi}_{\rm gg}^{\rm 2h}(r_0) = 1$.

As pointed out in Section 2, the correlation functions obtained by Norberg et al. (2001) have not been corrected for possible redshift evolution. This implies that the $r_0(L)$ measurements do not correspond to $z = 0$. In fact, since more luminous galaxies can be detected out to higher redshift, the correlation lengths of brighter galaxies correspond to galaxy populations with a higher median redshift. Note that the luminosities *have* been corrected to $z = 0$, and the LF used therefore corresponds to galaxies at the present time. Thus, in order to compare model and observations in a consistent

way, we calculate the model LF at $z = 0$ and the correlation function at some characteristic redshift of the sample in consideration. As an approximation, we estimate the mean redshift $\bar{z}$ for each volume-limited sample in Norberg et al. (2001), and calculate an effective bias factor $b_{\rm eff}(\bar{z})$ at this redshift from the bias factor b for $z = 0$ given by equation (29). Assuming that the number of galaxies is conserved in the redshift interval covered by the 2dFGRS ($\Delta z \sim 0.3$ for the brightest sample, and smaller for fainter samples), one can show that these two bias factors are related by

$$b_{\rm eff}(\bar{z}) = 1 + [D(0)/D(\bar{z})](b - 1), \tag{35}$$

(Mo & White 1996, 2002; Fry 1996) where $D(z)$ is the linear growth rate at redshift z, related to the linear growth factor $g(z)$ by $D(z) = g(z)/(1 + z)$. We use this effective bias factor and the mass correlation function at the mean redshift $\bar{z}$ to calculate the correlation length r_0 for each luminosity sample. For all the magnitude samples used here, the effect is modest, amounting to $\lesssim$10 per cent change in r_0.

3.3.2 The 1-halo term

For small separations, where the number of pairs are mostly due to galaxies in individual haloes, $\xi_{\rm gg}(r)$ depends not only on the occupation number of galaxies, but also on how galaxies are distributed in individual haloes.

To model the galaxy distribution in individual haloes, we assume that each halo contains one central galaxy (with luminosity $L_{\rm c}$, see equation 15) which is located at the halo centre. The other galaxies, which we call satellite galaxies, are distributed with a number density profile that is identical to the density profile of the dark matter (equation 33). This is clearly a simple assumption, because processes such as dynamical friction may lead to some segregation between galaxies and dark matter particles.

If the luminosity of the central galaxy $L_{\rm c} \in [L_1, L_2]$, the total number of pairs between the central galaxy and satellite galaxies in a halo of mass M is equal to the total number of satellite galaxies in the given luminosity range, $N_{\rm cs} = N_{\rm s}(M)$; otherwise (i.e. when $L_{\rm c}$ is not in $[L_1, L_2]$) this number is zero. The total number of distinct pairs of satellite galaxies is $N_{\rm ss} = \frac{1}{2}N_{\rm s}(N_{\rm s} - 1)$. The distribution of pair separations between central and satellite galaxies, which we denote by $f_{\rm c}(r)\,{\rm d}r$, has the NFW form. The satellite–satellite pairs follow a different distribution of separations, denoted by $f_{\rm s}(r)\,{\rm d}r$, which can be determined from the NFW density profile. The total number of galaxy pairs with separations in the range $r \pm {\rm d}r/2$ can thus be written as

$$N_{\rm pair}(M) f(r) = N_{\rm ss}(M) f_{\rm s}(r) + N_{\rm cs}(M) f_{\rm c}(r), \tag{36}$$

where

$$N_{\rm pair}(M) = \frac{1}{2}\langle N(M)(N(M) - 1)\rangle \tag{37}$$

is the total number of galaxy pairs regardless of separation, and $f(r)$ is determined through equation (26). The 1-halo term of the galaxy correlation function can then be estimated from

$$\frac{\bar{n}_{\rm g}^2}{2}\xi_{\rm gg}^{\rm 1h}(r) 4\pi r^2\,{\rm d}r = {\rm d}r \int n(M)\langle N_{\rm pair}(M)\rangle f(r)\,{\rm d}M, \tag{38}$$

where $\langle N_{\rm pair}(M)\rangle$ is the mean number of pairs in haloes of mass M (see Berlind & Weinberg 2002, for a similar approach).

Note that $\langle N_{\rm pair}(M)\rangle$ depends not only on the mean occupation $\langle N(M)\rangle$, but also on the second moment. Thus, in general, the 1-halo term depends also on the deviation of the occupation number from the mean. This deviation depends on the details of galaxy formation (e.g. Kauffmann et al. 1999; Benson et al. 2000). As a simple model, we make the assumption that $N(M)$ has the probability of $N + 1 - \langle N(M)\rangle$ to take the value N and the probability of $\langle N(M)\rangle - N$ to take the value $N + 1$, if $N < \langle N(M)\rangle < N + 1$. In this case, the mean number of pairs is[3]

$$\langle N_{\rm pair}\rangle = N\langle N\rangle - \frac{1}{2}N(N + 1) \tag{39}$$

This particular model for the distribution of halo occupation numbers is supported by the semi-analytical models of Benson et al. (2000), who found that the halo occupation probability distribution is narrower than a Poisson distribution with the same mean. In addition, Berlind & Weinberg (2002) have shown that distributions narrower than Poisson are more successful in yielding power-law correlation functions.

We use the 1-halo term only to investigate the *shape* of $\xi_{\rm gg}(r)$, not to compute r_0. Since the 1-halo term depends on, and is rather sensitive to, the assumptions about the distribution of galaxies inside dark matter haloes, we primarily focus on $r_0(L)$ and only briefly discuss the shape of $\xi_{\rm gg}(r)$ in Section 4.3.

4 RESULTS

Having specified the model and the observational constraints we now proceed as follows. After choosing a cosmological model, which sets the mass function $n(M)\,{\rm d}M$ and the two-point correlation function $\xi_{\rm hh}(r)$ of dark matter haloes, we specify the conditional LF $\Phi(L \mid M)$ and compute the LF $\hat{\Phi}(L)$ and correlation lengths $\hat{r}_0(L)$ of the model, using equations (1) and (29), respectively. Note that in all cases discussed here the correlation lengths, defined through $\xi_{\rm gg}(r_0) = 1$, are completely determined by the 2-halo term $\xi_{\rm gg}^{\rm 2h}(r)$ [i.e. $\hat{r}_0(L)$ is independent of our model for the distribution of galaxies in individual dark matter haloes]. Using Powell's multidimensional direction set method (e.g. Press et al. 1992), we find the values of $(M/L)_0$, M_1, β, γ_2 and η that minimize

$$\chi^2 = \chi^2(\Phi) + \chi^2(r_0). \tag{40}$$

Here

$$\chi^2(\Phi) = \sum_{i=1}^{N_\Phi}\left[\frac{\hat{\Phi}(L_i) - \Phi(L_i)}{\Delta\Phi(L_i)}\right]^2, \tag{41}$$

and

$$\chi^2(r_0) = \sum_{i=1}^{N_r}\left[\frac{\hat{r}_0(L_i) - r_0(L_i)}{\Delta r_0(L_i)}\right]^2, \tag{42}$$

with $N_\Phi = 35$ and $N_r = 8$ the number of data points for the LF and the correlation lengths, respectively.

Note that with this definition of χ^2, we are implicitly assigning the same weights to the measurements of $\Phi(L)$ and $r_0(L)$. This would be correct if there were no systematics in the measurements and if the error properties are the same in both cases. It is difficult to judge whether this is true in the present data, and so our definition of χ^2 is somewhat arbitrary. For instance, since $N_\Phi > N_r$ and since the errors on $\Phi(L)$ are typically much smaller than the errors on $r_0(L)$,

[3] Note: Berlind & Weinberg (2002), using the same model, adopted $\langle N_{\rm pair}\rangle = \langle N\rangle(\langle N\rangle - 1)$. This is only approximately correct and can lead to small errors for individual haloes with $\langle N\rangle \lesssim 5$. For the computation of $\xi_{\rm gg}(r)$, however, this approximation is sufficiently accurate.

Table 1. Model parameters for the ΛCDM 'concordance' model.

ID (1)	$\log M_L$ (2)	$(M/L)_{\rm cl}$ (3)	α_{15} (4)	$\log M_1$ (5)	$\log M_2$ (6)	$(M/L)_0$ (7)	β (8)	γ_1 (9)	γ_2 (10)	η (11)	$\chi^2(\Phi)$ (12)	$\chi^2(r_0)$ (13)	$\xi_{\rm gg}$ (14)
M1	13.5	500	−1.32	11.27	11.73	134	0.77	0.32	0.65	− 0.50	41.6	5.4	+
M1a	13.5	500	−1.32	11.34	11.73	133	0.75	0.33	0.65	− 0.50	41.4	5.8	+
M1b	13.5	500	−1.32	10.62	11.77	145	0.96	0.25	0.66	− 0.53	90.0	2.2	+
M1c	13.5	500	−1.32	11.88	11.25	79	0.46	0.52	0.63	− 0.65	54.5	3.0	+
M1d	13.5	500	−1.32	10.42	11.74	102	0.60	0.28	0.69	− 0.36	40.9	1.9	+
M1A	**12.5**	500	−1.32	8.64	12.60	163	2.81	0.15	0.83	−0.12	46.1	26.2	+
M1B	**14.5**	500	−1.32	12.82	12.19	111	0.56	0.80	0.87	−0.31	196.5	43.9	−
M1C	13.5	**250**	−1.32	10.37	12.60	325	1.21	0.05	0.73	−0.26	54.3	96.1	±
M1D	13.5	**750**	−1.32	11.81	11.49	111	0.57	0.52	0.63	−0.64	44.2	3.1	+
M1E	13.5	500	**−1.12**	11.06	11.93	136	1.07	0.29	0.72	−0.31	36.0	4.7	−
M1F	13.5	500	**−1.52**	11.46	11.53	133	0.64	0.34	0.60	−0.70	49.2	6.6	−
M1x	13.5	500	−1.32	11.53	11.74	141	0.77	0.34	0.64	− 0.50	143.0	7.2	+
M1y	13.5	500	−1.32	11.18	11.78	151	0.84	0.29	0.64	− 0.50	97.0	4.5	+
M1z	13.5	500	−1.32	11.23	11.75	147	0.81	0.30	0.64	− 0.51	109.9	6.1	+

Column (1) lists the ID by which we refer to each model in the text. Columns (2) to (4) list model parameters that are kept fixed; here M_L is defined such that $\tilde{L}^*(M_L) = L^*$, $(M/L)_{\rm cl}$ is the mass-to-light ratio of haloes with $M \geqslant 10^{14}\,h^{-1}\,{\rm M}_\odot$, and α_{15} is the faint-end slope of the conditional LF for haloes with $M = 10^{15}\,h^{-1}\,{\rm M}_\odot$. Columns (5) to (11) list the best-fitting model parameters, of which M_2 and γ_1 are set by M_L and $(M/L)_{\rm cl}$, respectively. Columns (12) and (13) list the values of $\chi^2(\Phi)$ and $\chi^2(r_0)$ of the best-fitting model, respectively. Finally, column (14) indicates whether the shape of the galaxy correlation functions are in good (+), reasonable (±) or poor (−) agreement with the data. Masses and mass-to-light ratios are in $h^{-1}\,{\rm M}_\odot$ and $h{\rm M/L}_\odot$, respectively.

Table 2. Model parameters for different cosmologies.

ID (1)	Ω_0 (2)	Ω_Λ (3)	σ_8 (4)	n (5)	R_f (6)	m_X (7)	$\log M_1$ (8)	$\log M_2$ (9)	$(M/L)_0$ (10)	β (11)	γ_1 (12)	γ_2 (13)	η (14)	$\chi^2(\Phi)$ (15)	$\chi^2(r_0)$ (16)	$\xi_{\rm gg}$ (17)
M2	**0.2**	0.8	**1.06**	1.0	–	–	11.25	11.18	72	0.6 0	0.42	0.64	−0.73	60.5	72.4	+
M3	**0.3**	0.7	**0.86**	1.0	–	–	11.42	11.69	132	0.7 2	0.34	0.65	−0.52	41.6	2.5	+
M4	**0.4**	0.6	**0.74**	1.0	–	–	11.10	12.16	226	1.0 2	0.22	0.66	−0.40	45.8	12.9	+
M5	**0.5**	0.5	**0.66**	1.0	–	–	10.92	12.58	369	1.4 0	0.14	0.69	−0.31	45.9	42.9	+
M6	**1.0**	0.0	**0.46**	1.0	–	–	8.74	14.34	5674	2.8 9	-0.14	0.83	−0.09	305.4	187.0	+
M7	0.3	0.7	**0.80**	1.0	–	–	11.66	11.62	127	0.64	0.38	0.64	−0.55	42.3	1.1	+
M8	0.3	0.7	**0.70**	1.0	–	–	12.40	11.49	120	0.46	0.57	0.61	−0.61	45.7	3.5	+
M9	0.3	0.7	0.90	**0.8**	–	–	11.32	11.57	110	0.70	0.36	0.65	−0.55	44.1	28.2	+
M10	0.3	0.7	0.90	**1.2**	–	–	11.20	11.88	160	0.84	0.28	0.66	−0.46	41.2	3.3	+
W1	0.3	0.7	0.90	1.0	**0.1**	0.8	10.93	11.64	118	0.6 4	0.30	0.66	−0.52	40.7	8.4	+
W2	0.3	0.7	0.90	1.0	**0.2**	0.5	10.00	11.37	70	0.2 5	0.29	0.68	−0.55	48.4	10.2	±

Column (1) lists the ID by which we refer to each model in the text. Models whose ID starts with M (W) correspond to CDM (WDM) models. Columns (2) to (5) indicate the parameters of the cosmological model, where the values modified with respect to the fiducial model (the ΛCDM concordance model) are in bold face. Columns (6) and (7) indicate the free streaming scale (in h^{-1} Mpc) and the dark matter particle mass (in keV), respectively (for WDM models only). Columns (8) to (17) are the same as columns (5) to (14) in Table 1.

the χ^2 minimization routine gives much more weight to fitting the LF than to fitting the correlation lengths. We will therefore also consider different relative weights for the LF and correlation length measurements, and only use χ^2 to assess the *relative* goodness-of-fit of different models. Tables 1 and 2 list the parameters for each model that we discuss in the text, together with the corresponding values for $\chi^2(\Phi)$ and $\chi^2(r_0)$.

Before proceeding, it is important to address the assumptions underlying the method. In addition to the trivial implicit assumption that all galaxies live inside dark matter haloes, we have assumed that (i) $\Phi(L \mid M)$ can be represented by a Schechter function, and (ii) $\Phi(L \mid M)$ is independent of environment; i.e. it is assumed that the galaxy properties inside a halo of mass M do not statistically depend on the halo's larger scale environment (this assumption only influences the estimates of $r_0(L)$, not the fitting of the LF). Although assumption (i) is supported by the fact that the LFs of groups and clusters of galaxies are reasonably well fitted by a Schechter function (e.g. Muriel et al. 1998; Beijersbergen et al. 2002; Trentham & Hodgkin 2002), there is no strong motivation for adopting a Schechter form for haloes of much lower mass. On the other hand, the Schechter function has a reasonable amount of freedom (it is specified by three free parameters), and we have tested in great detail that our results are robust against different parametrizations of these free parameters. Nevertheless, the validity of assumption (i) merits more detailed tests, which we intend to address in a future paper. Assumption (ii) is supported by the work of Lemson & Kauffmann (1999) who used numerical simulations to show that the properties of haloes of given mass, such as angular momentum and concentration, do not significantly depend on environment, and by the extended Press–Schechter formalism (e.g. Lacey & Cole 1993)

which predicts that the merging history of a halo of a given mass is independent of its large-scale environment. This assumption can ultimately be tested once better statistical samples of galaxies become available.

4.1 The concordance model

We first consider the standard ΛCDM model with $\Omega_0 = 0.3$, $\Omega_\Lambda = 0.7$, $h = 0.7$, $\Gamma = \Omega_0\, h = 0.21$, and $\sigma_8 = 0.9$. These cosmological parameters are consistent with a wide range of observations, and so this cosmology has become known as the 'concordance' model (e.g. Perlmutter et al. 1999; Riess et al. 1998, 2001; Melchiorri et al. 2000; de Bernardis et al. 2002).

The solid curves in Fig. 4 show the results for the best-fitting model (M1) for this concordance cosmology. Hereafter we refer to this model as our 'fiducial' model, and compare other models with respect to it. The bottom left panel compares the model LF with that of the 2dFGRS (open circles with error bars). The agreement is excellent, which is also apparent from the fact that $\chi^2(\Phi)$ divided by the number of degrees of freedom is very close to unity. The agreement with the observed $r_0(L)$ (shown in the bottom panel on the right) is also acceptable, although the model predicts slightly too large correlation lengths for galaxies with $M_{b_j} - 5\log h \gtrsim -20$. Note that the functional form of $r_0(L)$ is remarkably well reproduced by the model.

The best-fitting value of η is -0.50, which indicates that $\tilde{\alpha}$ decreases with increasing mass. Larger values of $\tilde{\alpha}$ imply a LF that is more peaked at around $\tilde{L}^*$, i.e. with relatively fewer galaxies with $L < \tilde{L}^*$. Note that a faint-end slope that decreases with increasing mass is at least qualitatively consistent with observational results (e.g. Trentham & Hodgkin 2002). The top left panel of Fig. 4 plots the characteristic luminosity, $\tilde{L}^*$, as function of mass. A best-fitting value for β of 0.77 implies that $\tilde{L}^* \propto M^{1.77}$ for $M \ll M_1 \simeq 1.9\times10^{11}\, h^{-1}\,\mathrm{M}_\odot$. The slope of $\tilde{L}^*(M)$ for haloes with $M \gg M_1$ is mainly controlled by γ_2, and is strongly constrained by the form of $r_0(L)$; larger (smaller) values of γ_2 cause $r_0(L)$ to

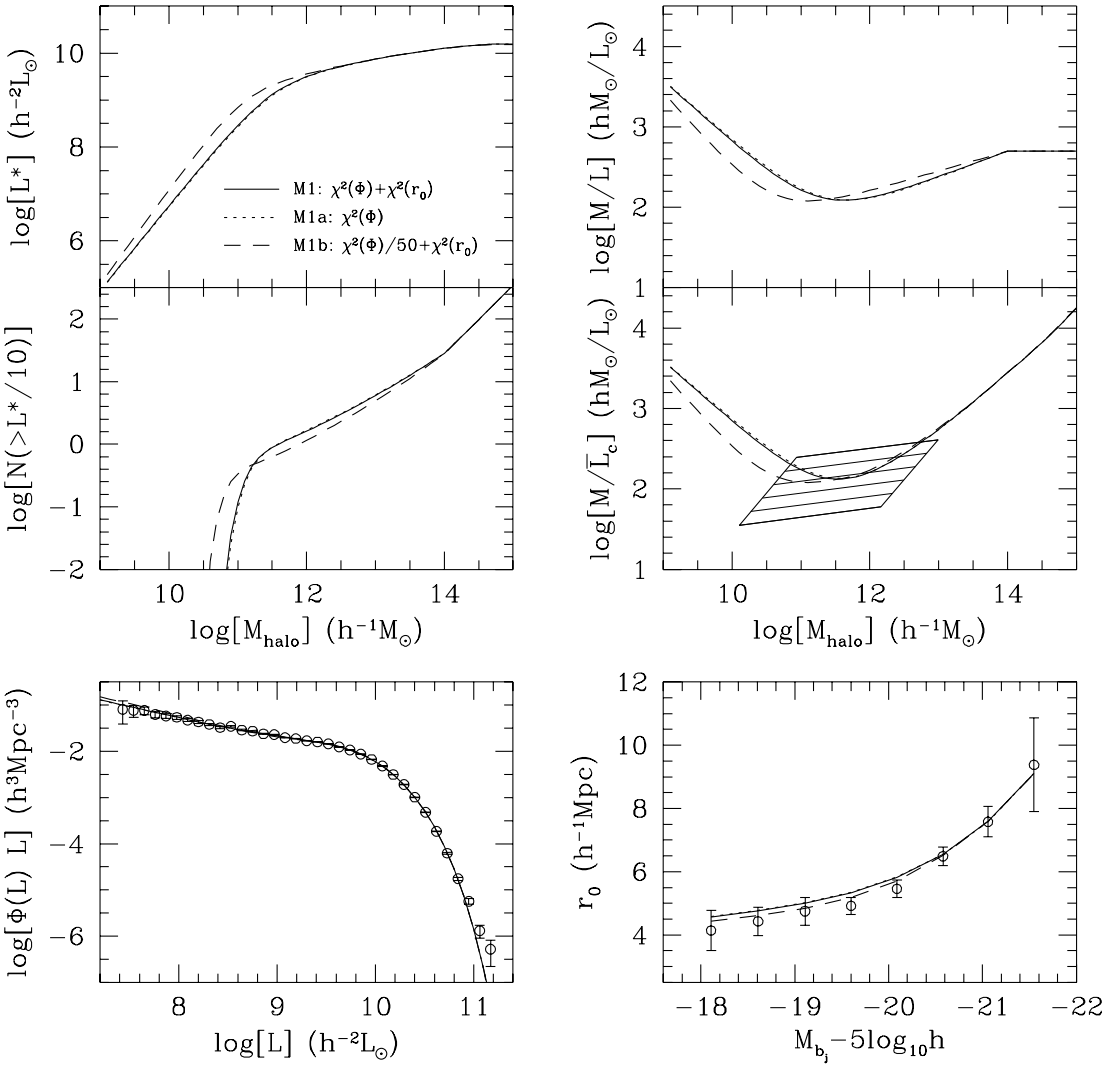

Figure 4. Results for the fiducial model M1 (solid lines). The two bottom panels compare the model predictions with the observed LF $\Phi(L)$ (left) and correlation lengths $r_0(L)$ (right). Open circles with error bars correspond to the 2dFGRS data from Norberg et al. (2001, 2002). The four top panels show, clockwise from the upper left panel, the characteristic luminosity, $\tilde{L}_\star$, the ratio between halo mass and total luminosity M/L, the ratio between halo mass and luminosity of the 'central' galaxy $M/\bar{L}_\mathrm{c}$, and the number of galaxies with $L > L^*/10$, all as function of halo mass. The dotted and dashed curves show the results obtained by minimizing $\chi^2 = \chi^2(\Phi)$ (Model M1a) and $\chi^2 = \chi^2(\Phi)/50 + \chi^2(r_0)$ (Model M1b), respectively.

increases less (more) rapid with increasing luminosity. Note that for our best-fitting value of $\gamma_2 = 0.65$ the value of $\bar{L}^*$ only increases by a factor $\sim$5 from $M = 10^{12}\,h^{-1}\,\mathrm{M}_\odot$ to $M = 10^{15}\,h^{-1}\,\mathrm{M}_\odot$.

The middle panel on the left plots $N(>L^*/10)$, the average number of galaxies brighter than one-tenth of the characteristic luminosity L^* of the 2dFGRS. For $M \gtrsim 10^{12}\,h^{-1}\,\mathrm{M}_\odot$, this number increases roughly linearly with mass, while below $\sim 10^{11}\,h^{-1}\,\mathrm{M}_\odot$ one basically no longer finds galaxies as bright as $L^*/10$. The top and middle panels on the right plot the mass-to-light ratios M/L and $M/\bar{L}_\mathrm{c}$, respectively. Here L is the average total luminosity of galaxies in a halo of mass M (see equation 2), and $\bar{L}_\mathrm{c}$ corresponds to the average luminosity of the 'central galaxy' (equation 15). The mass-to-light M/L reaches a minimum value of $\sim 125\,h\,\mathrm{M}/\mathrm{L}_\odot$ at $M \sim 10^{11.5}\,h^{-1}\,\mathrm{M}_\odot$. For haloes with masses smaller or larger than $\sim 10^{11.5}\,h^{-1}\,\mathrm{M}_\odot$, the galaxy formation efficiency is reduced, consistent with the fact that feedback can reduce the star formation efficiency in small haloes, while cooling becomes less effective in more massive haloes (e.g. White & Rees 1978; Dekel & Silk 1986; van den Bosch 2002; Benson et al. 2000). Note that, by construction, the mass-to-light ratio stays constant at $M/L = 500\,h\,\mathrm{M}/\mathrm{L}_\odot$ for $M \geqslant 10^{14}\,\mathrm{M}_\odot$ (see Section 3.2).

For low-mass haloes, the ratio $M/\bar{L}_\mathrm{c}$ has properties similar to M/L. This is a result of the fact that, by construction, each of these haloes hosts only one dominant ('central') galaxy. For massive systems, the faint-end slope of the conditional LF is steeper and $\mathcal{N}^* > 1$, causing $M/\bar{L}_\mathrm{c} > M/L$. The parallelogram indicates the TF constraints for six different values of $V_\mathrm{max}/V_\mathrm{vir}$ from 1.0 (upper line) to 2.0 in steps of 0.2 (see Fig. 1). In order for model M1 to be consistent with the zero-point of the TF relation, the ratio $V_\mathrm{max}/V_\mathrm{vir}$ must be smaller than 1.4, which is only marginally consistent with CDM predictions, especially when the boosting effect of the baryonic matter is taken into account (see discussion in Section 2.3). In addition, the fact that $M/\bar{L}_\mathrm{c}(M)$ is quite strongly 'curved' over the mass range of the TF constraints implies that $V_\mathrm{max}/V_\mathrm{vir}$ needs to vary significantly, and in a fine-tuned fashion, with mass in order to yield a linear TF relation.[4] Thus although model M1 yields a reasonable fit to the LF and $r_0(L)$, it predicts values for $M/\bar{L}_\mathrm{c}$ that are slightly too high.

As pointed out before, by virtue of the definition of χ^2 used in the minimization routine, much more weight is given to fitting the LF than to fitting the correlation lengths. Consequently, the fits are expected to be controlled mainly by the LF constraints. To demonstrate this, the dotted curves in Fig. 4, corresponding to model M1a, show the results obtained when fitting only the LF, i.e. by setting $\chi^2 = \chi^2(\Phi)$. The fact that these curves are all very similar to our fiducial model (solid curves) confirms the above assertion. In addition, the dashed curves in Fig. 4, corresponding to model M1b, show the results obtained by setting $\chi^2 = \chi^2(\Phi)/50 + \chi^2(r_0)$, i.e. by reducing the weights of the $\Phi(L)$ measurements by a factor 50. Not surprisingly, this model fits the correlation lengths better but fits the LF slightly worse, at least according to the value of $\chi^2(\Phi)$. Whether or not the fit is acceptable depends on possible systematic errors in the observed $\Phi(L)$ which may be larger than the statistical errors used here. We return to the issue of systematic errors in Section 5.1.

[4] Note that the discrepancy for haloes with $M \gtrsim 10^{12}\,h^{-1}\,\mathrm{M}_\odot$ may not be a too serious problem, because their central galaxies may be predominantly ellipticals for which the TF relation does not apply.

4.2 Less restrictive models

The results presented above suggest that, for the cosmological concordance model, the conditional luminosity distribution obtained from the observed LF and the observed clustering strength as function of luminosity overpredicts the mass-to-light ratios implied by the Tully–Fisher relation. However, this assertion is only correct for our restricted set of parametrized models for $\Phi(L\,|\,M)$. The more general model for our conditional LF has nine, rather than five, free parameters. Although we have argued that four of these parameters can be fixed based on physical and observational constraints, we now address the impact these 'restrictions' have on our results.

In our fiducial model we fix the mass M_2 by setting $M_L = 10^{13.5}\,h^{-1}\,\mathrm{M}_\odot$, where M_L is defined so that $\bar{L}^*(M_L) = L^*$. This choice is motivated by the fact that L^* does not seem to vary much over the range $10^{13}\,h^{-1}\,\mathrm{M}_\odot \lesssim M \lesssim 10^{15}\,h^{-1}\,\mathrm{M}_\odot$. To illustrate the impact that this assumption has on our results, the upper panels of Fig. 5 plot the results for models M1A and M1B where we set $M_L = 10^{12.5}\,h^{-1}\,\mathrm{M}_\odot$ and $M_L = 10^{14.5}\,h^{-1}\,\mathrm{M}_\odot$, respectively. Note that increasing (decreasing) the value of M_L mainly causes bright galaxies to reside in less (more) massive haloes. As one can see, the results depend quite sensitively on the value of M_L. For $M_L \gg 10^{13.5}\,h^{-1}\,\mathrm{M}_\odot$ the predicted $r_0(L)$ only shows a very mild luminosity dependence, in clear disagreement with the data. In addition, this model yields values of $\chi^2(\Phi)$ that are too high and predicts galaxy–galaxy correlation functions that deviate strongly from the power-law form for $M_{b_j} - 5\log h \lesssim -21.0$ (see Section 4.3 below). Model M1A, for which $M_L = 10^{12.5}\,h^{-1}\,\mathrm{M}_\odot$, also fails to match the observed $r_0(L)$ for bright galaxies. Both models predict mass-to-light ratios that are clearly inconsistent with the TF constraints. We therefore conclude that models with $10^{13}\,h^{-1}\,\mathrm{M}_\odot \lesssim M_L \lesssim 10^{13.5}\,h^{-1}\,\mathrm{M}_\odot$ are the most successful, and in what follows we keep M_L fixed at $10^{13.5}\,h^{-1}\,\mathrm{M}_\odot$.

In the fiducial model, we tune γ_1 so that $M/L = (M/L)_\mathrm{cl} = 500\,h\,\mathrm{M}/\mathrm{L}_\odot$ at $M = 10^{14}\,h^{-1}\,\mathrm{M}_\odot$, and we keep M/L fixed at the value of $(M/L)_\mathrm{cl}$ for more massive systems. The middle two panels of Fig. 5 show the effects of changing $(M/L)_\mathrm{cl}$ to 250 h $\mathrm{M}/\mathrm{L}_\odot$ (model M1C) and $750\,h\,\mathrm{M}/\mathrm{L}_\odot$ (model M1D). These values are still consistent with the observational constraints of Fukugita et al. (1998) at the $3\,\sigma$ level. Increasing (decreasing) $(M/L)_\mathrm{cl}$ causes a decrease (increase) of the number of galaxies in massive haloes. Since the clustering strength of haloes increases with mass, an increase (decrease) of $(M/L)_\mathrm{cl}$ therefore results in lower (higher) values of $r_0(L)$. For $(M/L)_\mathrm{cl} < 500\,h\,\mathrm{M}/\mathrm{L}_\odot$ the models predict too large correlation lengths as well as mass-to-light ratios that are inconsistent with the TF constraints. Model M1D, however, predicts a $\hat{r}_0(L)$ and $\hat{\Phi}(L)$ that are both in agreement with the data. Over the mass range probed by the TF constraints, the mass-to-light ratios are almost identical to those of the fiducial model; they are slightly too high and reveal an uncomfortably large variation over this mass range. Since $(M/L)_\mathrm{cl} = 750\,h\,\mathrm{M}/\mathrm{L}_\odot$ is only marginally consistent with the observational constraints of Fukugita et al. (1998), we restrict ourselves to $(M/L)_\mathrm{cl} = 500\,h\,\mathrm{M}/\mathrm{L}_\odot$ in what follows.

The lower panels of Fig. 5 compare the fiducial model (for which $\alpha_{15} = -1.32$) with models M1E and M1F for which $\alpha_{15} = -1.12$ and $\alpha_{15} = -1.52$, respectively. The choice of α_{15} has only a small impact on the results. A change in α_{15} is largely compensated by changes in M_1, β and η, but does not significantly improve or worsen the agreement with the data. However, α_{15} does impact on the shape of $\xi_\mathrm{gg}(r)$ (see Section 4.5 below) with $\alpha_{15} = -1.32$ clearly giving the best results. We therefore restrict ourselves to models with $\alpha_{15} = -1.32$ in what follows.

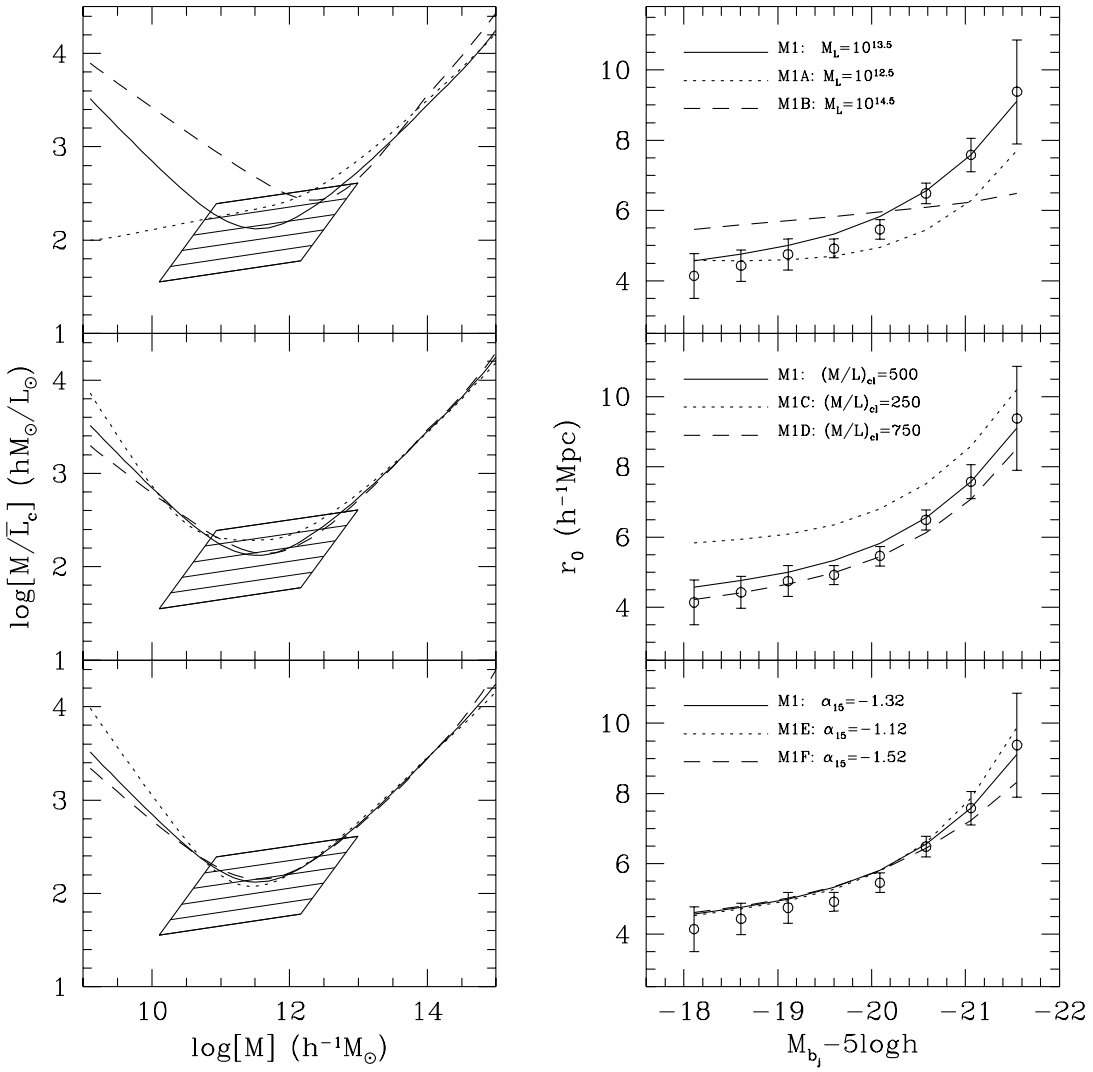

Figure 5. Results of models in which one model parameter is changed relative to the fiducial choice. Left panels show $M/\bar{L}_c$ as a function of halo mass (parallelogram indicates the TF constraints), while the right panels show the correlation length as a function of absolute magnitude. Open circles with error bars correspond to the observational data from the 2dFGRS. Solid curves in each panel correspond to the fiducial model M1. Top panels show results for models with $M_L = 10^{12.5}\,h^{-1}\,\mathrm{M}_\odot$ (Model M1A, dotted curves) and $M_1 = 10^{14.5}\,h^{-1}\,\mathrm{M}_\odot$ (Model M1B, dashed curves). Middle panels show results for models with $(M/L)_{\rm cl} = 250\,h\,\mathrm{M}/\mathrm{L}_\odot$ (Model M1C, dotted curves) and $(M/L)_{\rm cl} = 750\,h\,\mathrm{M}/\mathrm{L}_\odot$ (Model M1D, dashed curves). Bottom panels show results for $\alpha_{15} = -1.12$ (Model M1E, dotted curves) and $\alpha_{15} = -1.52$ (Model M1F, dashed curves). See text for a detailed discussion.

Finally we investigated the effect of changing $M_{\rm min}$, i.e. the mass scale below which $\Phi(L\,|\,M) = 0$. We find that as long as $M_{\rm min} \lesssim 10^{10}\,h^{-1}\,\mathrm{M}_\odot$ our results do not significantly depend on $M_{\rm min}$, and our fiducial value of $10^9\,h^{-1}\,\mathrm{M}_\odot$, which is motivated by reionization considerations, therefore does not influence any of the results presented here.

In addition to varying some of the parameters kept fixed in our fiducial models, we also experimented with completely different parametrized forms of $\tilde{L}^*$, $\tilde{\alpha}$, and $\tilde{\Phi}^*$. Neither of these alternative models, however, was able to yield results in better agreement with the data. Therefore, we conclude that the ΛCDM concordance model can be made consistent with both the observed LF and the correlation lengths as function of luminosity. The largest problem for the cosmological concordance model is to fit the zero-point of the TF relation. In all the models presented here, the mass-to-light ratios are only consistent with the TF constraints if $V_{\rm max}/V_{\rm vir} \lesssim 1.4$, which is hard to reconcile with typical CDM predictions (see discussion in Section 2.3). Probably equally problematic, is the fact that the models predict mass-to-light ratios that vary strongly over the mass range probed by the TF constraints.

4.3 The shape of the correlation function

It is well known that the observed correlation function of galaxies is well fitted by a single power law $\xi_{\rm gg}(r) = (r/r_0)^{-\gamma}$ over a wide range of radii (e.g. Davis & Peebles 1983; Baugh 1996; Jing et al. 1998; Zehavi et al. 2002). Norberg et al. (2001) have recently shown that even when $\xi_{\rm gg}(r)$ is split in several luminosity bins, each individual correlation function is still well fitted by a single power law with $\gamma \simeq 1.7$. These observations yield extra constraints on the conditional luminosity function. Note that the mass correlation function of the CDM model in consideration is *not* well described by a pure power law (see Fig. 3). The power-law behaviour of $\xi_{\rm gg}(r)$ for individual luminosity bins therefore results from some non-trivial

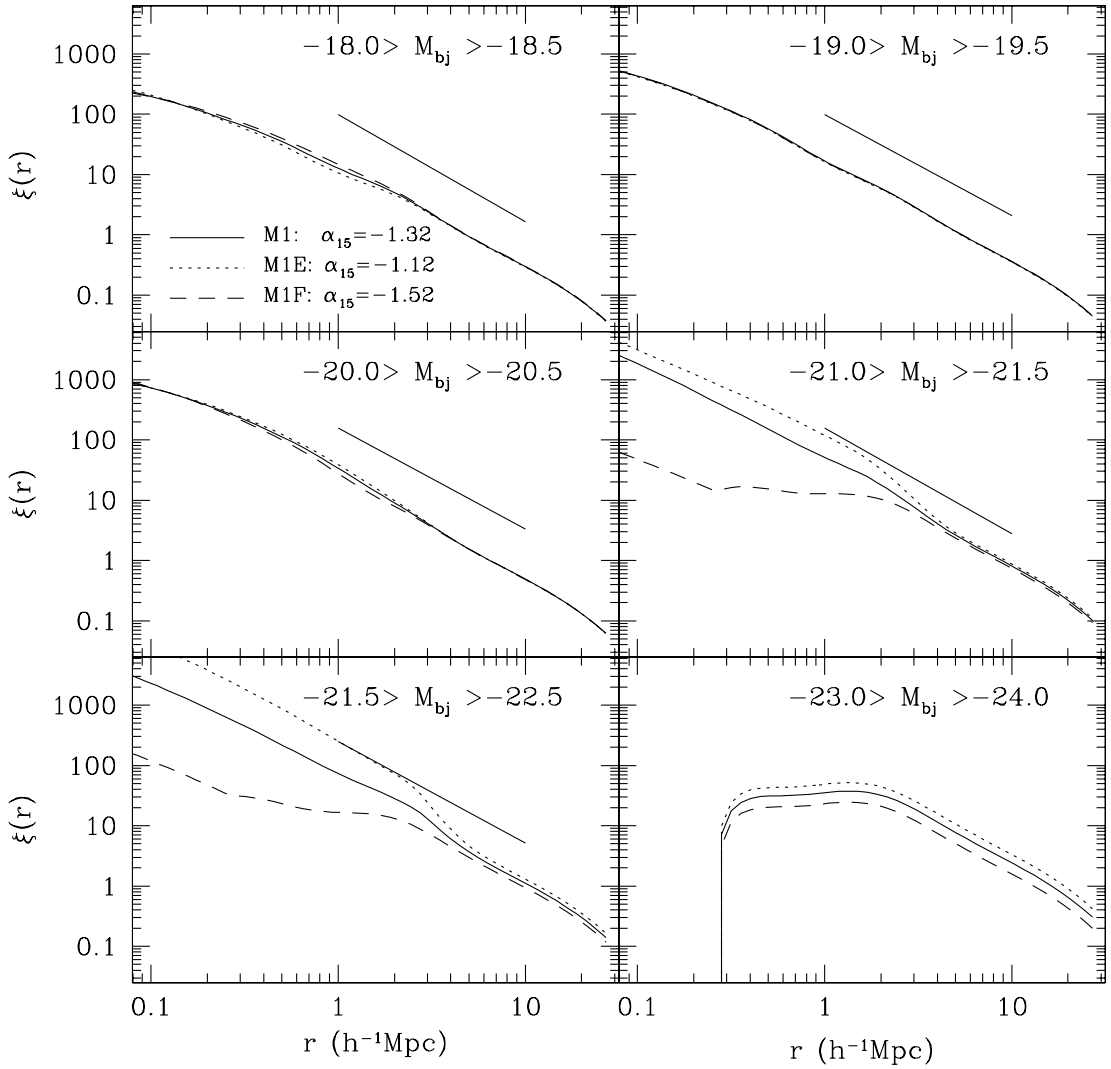

Figure 6. The predicted two-point correlation functions of galaxies in different absolute magnitude bins. Results are shown for the fiducial model (Model M1; solid curves), and for models M1E ($\alpha_{15} = -1.12$; dotted curves) and M1F ($\alpha_{15} = -1.52$; dashed curves). The short solid line-segments indicate the slopes of the best-fitting power laws obtained by Norberg et al. (2001) for 2dFGRS galaxies in the same magnitude bins. No such line-segment is shown in the lower right panel, since no 2dFGRS data are available for this magnitude bin. Note that the correlation functions of the fiducial model resemble power laws over the entire radial range plotted, with slopes that are very similar to those observed. An exception is the magnitude bin in the lower right panel, which reveals a clear deviation from a power law at small separations. Models M1E and M1F, on the other hand, show significant deviations from a pure power law behaviour for galaxies with $-21 > M_{b_j} - 5\log h > -22.5$.

conspiracy between the halo bias on large scales (the 2-halo term) and the distribution of galaxies within individual dark matter haloes (the 1-halo term) on small scales. This property of the galaxy occupation model has been noticed in some early investigations (e.g. Jing et al. 1998, 2002; Kauffmann et al. 1999; Benson et al. 2000; Berlind & Weinberg 2002).

Fig. 6 plots the galaxy–galaxy correlation functions of model M1 (solid lines) for five luminosity bins also used by Norberg et al. (2001). In addition, we also plot predictions for the magnitude bin $-24 < M_{b_j} - 5\log h < -23$. For all subsamples with $M_{b_j} - 5\log h > -22.5$, the correlation functions have roughly a power-law form over the entire range from $r \simeq 0.1\,h^{-1}$ Mpc to $r \simeq 20\,h^{-1}$ Mpc, and with a slope close to that measured from the 2dFGRS (indicated in each panel). For galaxies with $-23.0 > M_{b_j} - 5\log h > -24.0$, however, the correlation function is strongly suppressed at $r \lesssim 2\,h^{-1}$ Mpc. These bright galaxies correspond to the central galaxies of rich clusters, and so their correlation function contains only a negligible contribution from the 1-halo term. Unfortunately, the 2dFGRS results of Norberg et al. (2001) only considered galaxies with $M_{b_j} - 5\log h > -22.5$, so that we cannot compare this prediction with data. Fig. 6 also plots the predictions for models M1E ($\alpha_{15} = -1.12$) and M1F ($\alpha_{15} = -1.52$). Both these models show significant deviations from a single power-law form (at least for the brighter galaxies), demonstrating that the actual shape of the correlation function can be used to discriminate between different models for the conditional LF. It is remarkable that the model with $\alpha_{15} = -1.32$, which is the value obtained by Beijersbergen et al. (2002) for the Coma cluster, yields the best result.

Although the shapes of the two-point correlation functions of our fiducial model are in good agreement with the 2dFGRS, this success is model-dependent. In particular, we have assumed that the

distribution of galaxies in individual haloes follows the density distribution of dark matter, and we have made simplified assumptions regarding the second moment of the distribution of the halo occupation numbers. Indeed, as shown in Berlind & Weinberg (2002), the shape of the correlation function on small scales may depend sensitively on these assumptions, and a good power law is not always obtained. Therefore, in judging the success of our models we will not give too much weight to the actual shape of $\xi_{\rm gg}(r)$. For completeness, we *do* indicate in Tables 1 and 2 whether the correlation functions, obtained under the assumptions of our model for the 1-halo term, are in good (+), reasonable (±) or poor (−) agreement with the data.

4.4 An alternative sampling of the luminosities of central galaxies

So far our calculations are based on the assumption that the luminosity of the central galaxy of a halo is a random variable with the distribution function $\Phi(L\,|\,M)$ at $L > L_1$ (see Section 3.2). Although perfectly self-consistent, it may cause a large spread in $L_{\rm c}$ for haloes in which $L_1/\tilde{L}^*$ is small. This may be unrealistic in low-mass haloes where, according to numerical simulations and semi-analytic models (e.g. Katz et al. 1996; Fardal et al. 2001; Pearce et al. 2000; Kay et al. 2002; Kauffmann et al. 1993; Somerville & Primack 1999; Cole et al. 2000), central galaxies have a rather narrow luminosity distribution for given halo mass. We therefore consider an alternative distribution of $L_{\rm c}$. Inspecting the observed TF relation (Fig. 1), it seems that the luminosities of spiral galaxies with a given $V_{\rm max}$ follow a roughly log-normal distribution. We therefore modify the Schechter form of $\Phi(L\,|\,M)$ for haloes less massive than some value $M_{\rm c}$ by replacing the part with $L > L_1$ with a log-normal distribution

$$P(L_{\rm c})\,{\rm d}L_{\rm c} = \frac{1}{\sigma_{\rm c}\sqrt{2\pi}}\exp\left(-\frac{\log_{10}{}^2(L_{\rm c}/\bar{L}_{\rm c})}{2\sigma_{\rm c}^2}\right){\rm d}\log_{10}L_{\rm c}, \qquad (43)$$

which has a median $\bar{L}_{\rm c}$, given by equation (15), and a width $\sigma_{\rm c}$ which we treat as a free parameter. We are mainly interested to see whether this modification of $\Phi(L\,|\,M)$ can also fit the observational constraints, while yielding a $\sigma_{\rm c}$ that is roughly consistent with the observed scatter in the TF relation.

The spiral galaxies in the TF sample have masses in the range $10^{11.0}$ to $10^{12.5}\,h^{-1}\,{\rm M}_\odot$, and we therefore consider three values of $M_{\rm c}$: $10^{12.0}$, $10^{12.5}$, and $10^{13.0}\,h^{-1}\,{\rm M}_\odot$. For each of these values of $M_{\rm c}$ we derive the best-fitting parameters of the modified $\Phi(L\,|\,M)$ using $\sigma_{\rm c}$ as an additional free parameter, and setting the values of the fixed parameters to those of model M1. Results are shown in Fig. 7 (see Table 1 for the best-fitting parameters). As one can see, with $M_{\rm c} \sim 10^{12.5}\,h^{-1}\,{\rm M}_\odot$ the model fits the data reasonably well, and the parameters obtained are not very different from those in model M1. For the three choices of $M_{\rm c}$, $10^{12.0}$, $10^{12.5}$ and $10^{13.0}\,h^{-1}\,{\rm M}_\odot$, the best-fitting values of $\sigma_{\rm c}$ are 0.215, 0.203 and 0.168, respectively. These dispersions imply a TF scatter of ∼0.5 mag in good agreement with the observations. Thus, a simple modification of the conditional luminosity function can be found that results in a scatter in $L_{\rm c}$ consistent with the observed TF scatter.

5 SYSTEMATIC ERRORS IN THE OBSERVATIONAL CONSTRAINTS

As we have shown above, none of the ΛCDM concordance models is fully consistent with all observational constraints. Here we address whether this discrepancy might result from uncertainties and/or systematic errors in the observational constraints.

5.1 The luminosity function

The determination of an accurate LF is non-trivial. The accuracy depends, amongst others, on the size of the redshift survey (the larger the survey, the smaller the systematic errors due to large scale structure), on surface brightness completeness effects, on the accuracy of star–galaxy separation, and on the accuracy of the photometric calibration. In addition, corrections have to be made for band-shifting (the *k* correction) and for evolutionary effects of the galaxy population with redshift, each of which has its own uncertainties. Our main motivations for using the 2dFGRS LF are that (i) it is the largest extant redshift survey, (ii) its quoted errors have contributions from all the effects mentioned above, and, most importantly, (iii) the differential galaxy clustering properties, used as additional constraints on the model, have been derived from the same 2dFGRS data set.

Despite these advantages over other LFs available in the literature, one cannot rule out that some amount of systematic errors are present. For instance, Blanton et al. (2001) claim that the 2dFGRS LF (initially presented by Folkes et al. 1999) is inconsistent with the LF of the SDSS commissioning data. Norberg et al. (2002), however, claim that after taking account of zero-point photometric offsets, after correcting for galaxy evolution, and after making corrections for the proper conversion between SDSS and 2dFGRS magnitudes, both LFs are actually in good agreement.

Despite this apparent concordance, it is worthwhile to investigate how the presence of certain systematic errors impacts on our results. One of the most likely sources for systematic errors is incompleteness. Note that the incompleteness corrections applied by Norberg et al. were based on a comparison with the SDSS early-data release, which itself is not expected to be 100 per cent complete. If indeed the 2dFGRS suffers from incompleteness effect, the true luminosity densities will be higher, resulting in lower mass-to-light ratios for individual dark matter haloes. This is exactly the effect that might alleviate the problems with the TF constraints outlined above. We therefore address the impact incompleteness may have on our results using two different approaches.

First we consider an overall, luminosity-independent incompleteness, by assuming that Φ^* of the 2dFGRS is a factor 1.5 too small (Model M1c). Note that this is roughly similar to the disagreement between the SDSS and 2dFGRS LFs claimed by Blanton et al. (2001). Secondly we consider the possibility of a luminosity-dependent incompleteness by assuming that the true value of α is −1.4 rather than −1.21 (Model M1d). Results are shown in Fig. 8. Not surprisingly, both models result in mass-to-light ratios in better agreement with the TF relation. Thus, the ΛCDM concordance model can be made consistent with all observational constraints considered here if the 2dFGRS is only about 70 per cent complete at all luminosities. Given the discussion in Norberg et al. (2002) such extreme incompleteness effects, however, seem unlikely.

The incompleteness effects discussed here have exactly the same effect as the presence of dark CDM haloes (i.e. haloes in which no observable galaxies formed)[5]. In this case, model M1c is to be interpreted as a model in which one third of all haloes (independent of mass) host no observable galaxies (i.e. $\Phi(L\,|\,M) = 0$), while in the case of model M1d the fraction of dark CDM haloes increases with decreasing halo mass. The possibility of dark CDM haloes was recently discussed by Verde, Oh & Jimenez (2002), who argued that haloes with large angular momenta might result in discs of such low

[5] Note that we have already assumed that haloes with $M < M_{\rm min}$ are dark, which we associated with reionization effects.

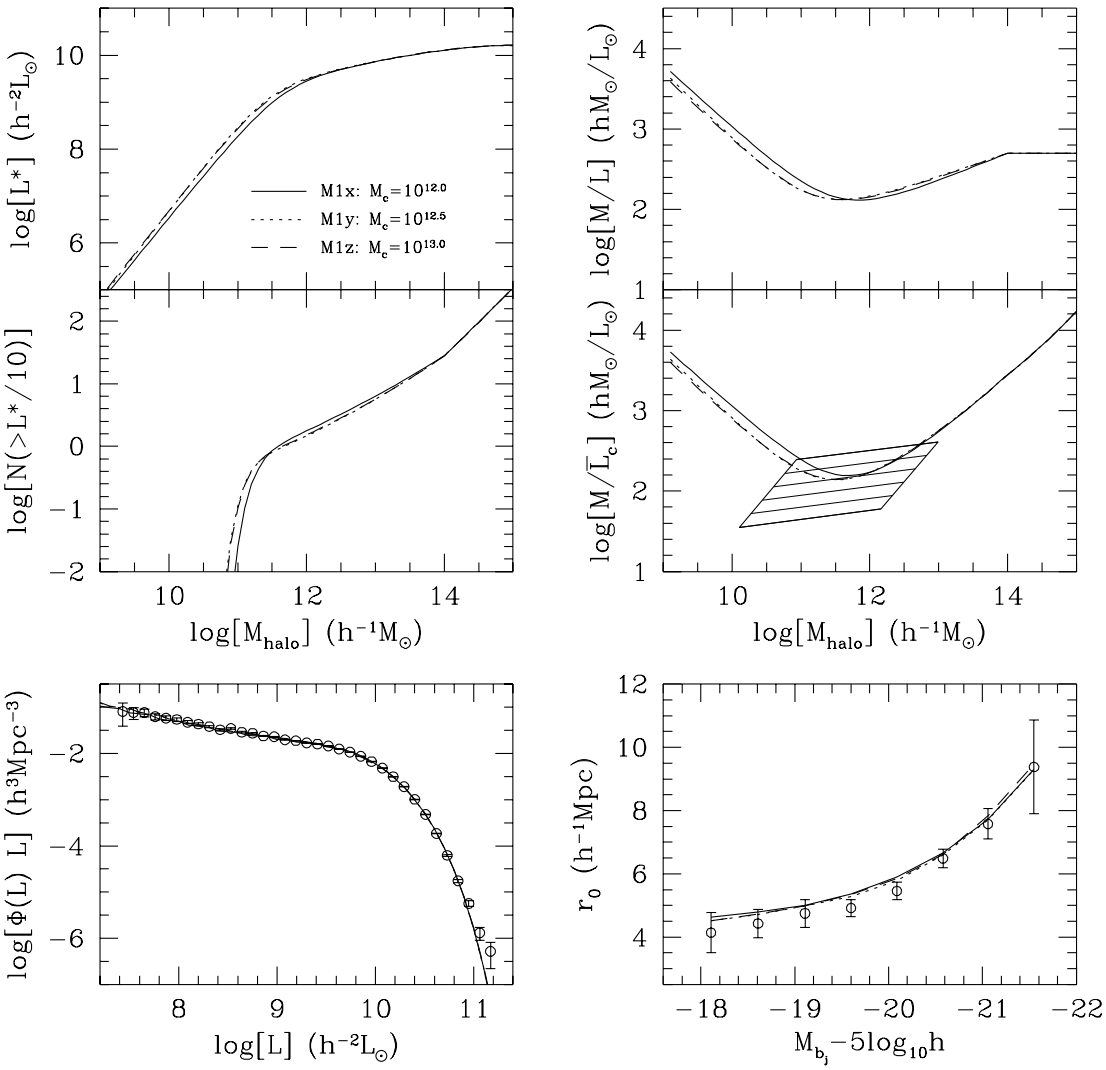

Figure 7. Same as Fig. 4 except that the luminosities of central galaxies in haloes with $M < M_c$ are sampled according to the log-normal model described in the text. The three curves correspond to $M_c = 10^{12.0}$ (solid), $M_c = 10^{12.5}$ (dotted) and $M_c = 10^{13.0}\,h^{-1}\,M_\odot$ (dashed), respectively. The model parameters used in the fitting are the same as in M1, these parameters and the parameters obtained from the fitting are listed in Table 1. The best-fitting values of the dispersion of the log-normal distribution, $\sigma_{\log L_c}$, are presented and discussed in the text.

surface brightness that star formation is never triggered (see also Jimenez et al. 1997). As shown by Jimenez, Verde & Oh (2002) a large abundance of dark CDM haloes is consistent with the rotation curves of disc galaxies. Based on our discussion above, we therefore conclude that the disagreement of the ΛCDM concordance model with the TF constraints may be alleviated if a relatively large fraction of dark matter haloes never managed to form observable galaxies.

5.2 The correlation lengths

As we have argued above, the differential clustering strength of galaxies as function of luminosity provides important additional constraints that allow us to obtain a unique best-fitting $\Phi(L\,|\,M)$. In particular, the value of γ_2 is strongly constrained by the strong increase in correlation length at the bright end.

In this paper, we used the results from the 2dFGRS, presented by Norberg et al. (2001), for the reasons already mentioned in Section 5.1. A comparison of the $r_0(L)$ obtained from the 2dFGRS with those obtained from a variety of other surveys, in particular the Southern Sky Redshift Survey 2 (Benoist et al. 1996; Willmer et al. 1998), the Stromlo/APM redshift survey (Loveday et al. 1995), and the ESO Slice Project (Guzzo et al. 2000), shows an overall agreement that $r_0(L)$ increases with increasing luminosity (see Fig. 3 in Norberg et al. 2001). Quantitatively, however, the disagreement is relatively large compared with the quoted error bars. Undoubtedly, to a large extent this owes to sampling fluctuations associated with the relatively small size of some of these surveys (e.g. Benson et al. 2001). Since the 2dFGRS is currently by far the largest redshift survey for which differential clustering measures have been obtained, we adhere to these data. In the near future, when the full 2dFGRS and SDSS results are available, the true accuracy of the $r_0(L)$ measurements used here can be addressed in more detail.

5.3 The Tully–Fisher zero-point

We have argued that the $M/\bar{L}_c$ of our fiducial model are at best marginally consistent with the (zero-point of) the TF relation. We computed our TF constraints from the data of TP00, for which the

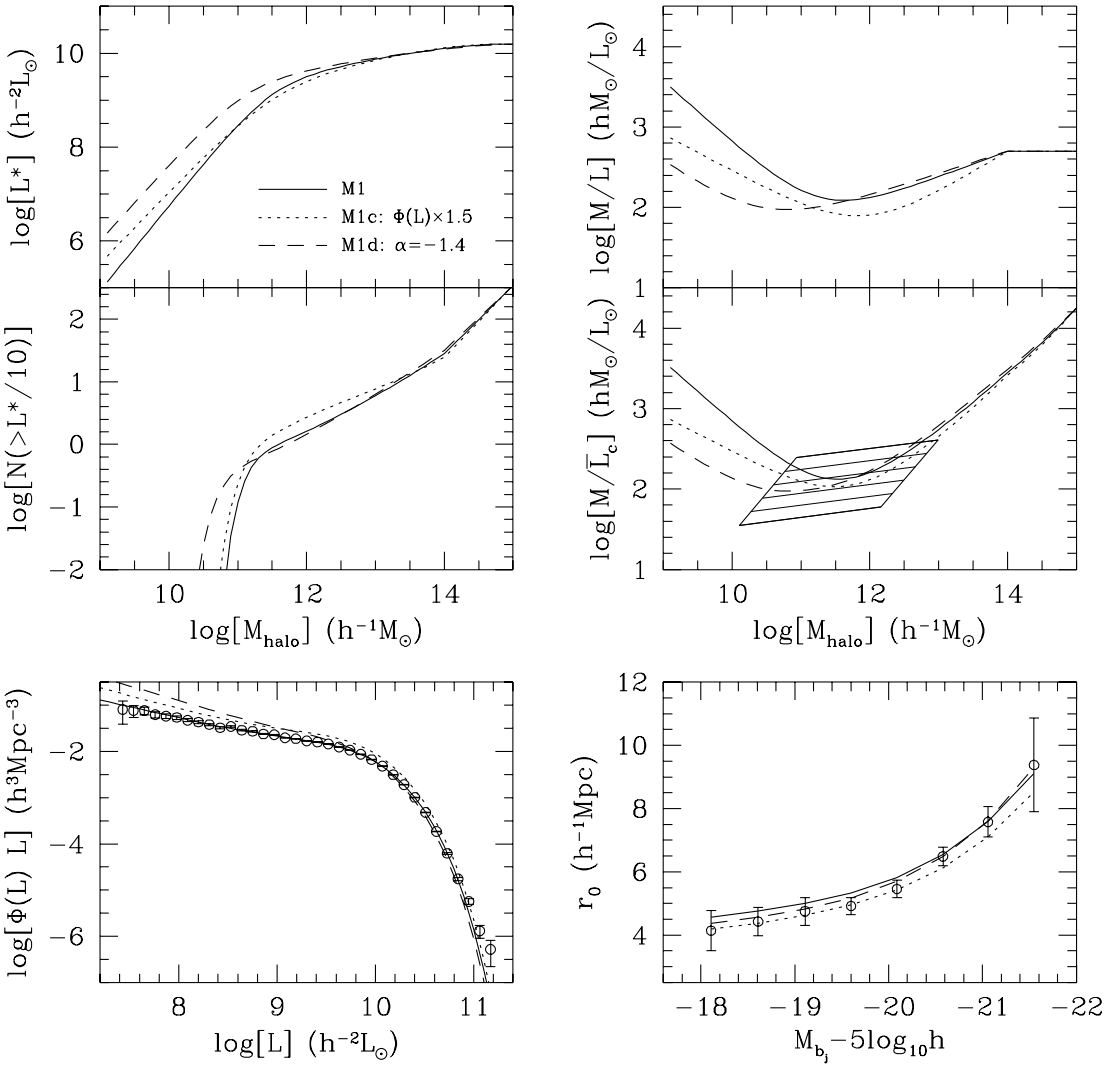

Figure 8. Same as Fig. 4 except that here we compare the fiducial model M1 with models in which we assume that the true LF differs from the 2dFGRS LF. In particular, we show results for models in which we assume that the true number density of galaxies is 1.5 times as high as for the 2dFGRS LF, independent of luminosity (Model M1c; dotted curves), and in which we assume that the true faint-end slope is $\alpha = -1.4$ in stead of -1.21 (Model M1d; dashed curves). Note that both models results in lower values of $M/\bar{L}_{\rm c}$ (in better agreement with the TF constraints) and in smaller correlation lengths (in better agreement with the 2dFGRS data).

absolute magnitudes have been determined using distances obtained with the Cepheid period-luminosity relationship. The zero-point of this TF relation therefore intrinsically contains an effective Hubble parameter. In order to be able to make a comparison with our models and with the data on the LF and the galaxy–galaxy clustering, we converted the absolute magnitudes of the TP00 data to $M_{b_j} - 5\log h$ adopting $H_0 = 70\,{\rm km\,s^{-1}\,Mpc^{-1}}$. This particular choice for the Hubble constant is motivated by (i) the value $H_0 = 72 \pm 8\,{\rm km\,s^{-1}\,Mpc^{-1}}$ (68 per cent confidence) obtained by the *HST* Key Project (Freedman et al. 2001), (ii) the value $H_0 = 77 \pm 8\,{\rm km\,s^{-1}\,Mpc^{-1}}$ (95 per cent confidence) obtained by TP00 from the same TF data used here, and (iii) the fact that we have adopted $h = 0.7$ in all our models.

However, some uncertainty regarding H_0 remains, and this will directly influence the normalization of the TF zero-point. For example, determinations of H_0 based on time-delay measurements of gravitational lenses usually yield values for the Hubble parameter that are significantly smaller (e.g. Kochanek 2002; but compare Hjorth et al. 2002). Kochanek (2002) obtains $H_0 = 48^{+7}_{-4}\,{\rm km\,s^{-1}\,Mpc^{-1}}$ (95 per cent confidence) under the assumption that the lenses have flat rotation curves. Furthermore, Saha et al. (2001), using Cepheid calibrations for a sample of galaxies with Type Ia supernovae, finds $H_0 = 59 \pm 6\,{\rm km\,s^{-1}\,Mpc^{-1}}$.

It is straightforward to correct our TF constraints for an error in H_0. The mass-to-light ratios obtained from equation (5) scale as

$$\log\left(\frac{M}{\bar{L}_{\rm c}}\right)_h = \log\left(\frac{M}{\bar{L}_{\rm c}}\right)_{0.7} - 2\log\left(\frac{h}{0.7}\right). \qquad (44)$$

Thus, for $h < 0.7$ the mass-to-light ratios obtained from the TP00 TF relation become larger. In other words, if for a given halo mass M and our assumption that $h = 0.7$ the $M/\bar{L}_{\rm c}$ of a model implies a value $(V_{\rm max}/V_{\rm vir})_{0.7}$, then for $h \neq 0.7$ the implied ratio is

$$\left(\frac{V_{\rm max}}{V_{\rm vir}}\right)_h = \left(\frac{V_{\rm max}}{V_{\rm vir}}\right)_{0.7} \times \left(\frac{h}{0.7}\right)^{-0.75}, \qquad (45)$$

where we have used $b_{\rm TF} = 2.67$ (see Section 2.3). For example, in our fiducial model (M1) the values of $M/\bar{L}_{\rm c}$ imply that $V_{\rm max}/V_{\rm vir} \lesssim 1.4$,

which is hard to reconcile with the typical circular velocity curves of CDM haloes. If, however, $h = 0.5$ then we obtain $V_{\rm max}/V_{\rm vir} \lesssim 1.8$, in much better agreement with CDM predictions.

6 COSMOLOGICAL CONSTRAINTS

So far we have only focused on the ΛCDM concordance cosmology. In the present section, we turn our attention to a number of alternative cosmologies to (i) investigate whether the method presented here can be used to constrain cosmological parameters and (ii) to see whether we can find a set of cosmological parameters that improves the fit to $\Phi(L)$ and $r_0(L)$ with respect to the concordance model while simultaneously yielding mass-to-light ratios that are in better agreement with the TF constraints.

In a recent study, Zheng et al. (2002) have shown that distinct cosmological models produce distinct halo populations. Based on a detailed investigation of halo populations in a wide range of cosmologies, Zheng et al. argued that a combination of galaxy clustering and statistics that are sensitive to the virial masses of dark matter haloes should be able to impose strong constraints on cosmological models without having to rely on a priori assumptions regarding galaxy formation. Indeed, recently Guzik & Seljak (2002) and Yang et al. (2002) used the galaxy–galaxy weak lensing results of the SDSS (McKay et al. 2001) to constrain the virial masses of galaxies brighter than L^* (see also McKay et al. 2002). Linking these results to the abundance of dark matter haloes, Seljak (2002b) was able to place useful constraints on cosmological parameters. This suggests that our combination of constraints from the luminosity-dependent clustering strengths and the mass-to-light ratios implied by the TF relation, should impose constraints on cosmological parameters. As we show below, this is indeed the case.

6.1 The matter density

We consider cosmologies in which the matter density is varied with respect to the concordance value $\Omega_0 = 0.3$ (models M2–M6; see Table 2). All models considered here have $\Omega_\Lambda = 1.0 - \Omega_0$, to keep agreement with the cosmic microwave background constraints (e.g. Melchiorri et al. 2000; de Bernardis et al. 2002), and we adopt $\Gamma = \Omega_0\, h$ throughout. In addition, when we modify Ω_0 we also change the normalization σ_8, in order to satisfy the weak lensing constraints obtained by Hoekstra, Yee & Gladders (2002):

$$\sigma_8 \Omega_0^{0.52} = 0.46. \qquad (46)$$

This allows us to investigate whether our modelling of the conditional LF can break the degeneracy between σ_8 and Ω_0 that results from weak lensing and cluster abundance measurements.

Comparing models with $\Omega_0 \neq 0.3$ with data is somewhat complicated by the fact that obtaining $\Phi(L)$ and $r_0(L)$ from observations is cosmology-dependent. The observational constraints used so far were obtained assuming $\Omega_0 = 0.3$ and $\Omega_\Lambda = 0.7$, consistent with the cosmological parameters considered up to this point. For other values of Ω_0 and Ω_Λ, however, the observational constraints from the 2dFGRS will be different. For the LF, S. Cole and P. Norberg kindly provided $\Phi(L)$ obtained from the 2dFGRS for the additional cosmologies considered here (private communications). For the $r_0(L)$, however, only measurements for $\Omega_0 = 0.3$ and $\Omega_\Lambda = 0.7$ are available to us (from Norberg et al. 2001). We therefore ignore the cosmology dependence of the observed correlation lengths in our analyses. Since the Ω_0 dependence is small compared with the statistical errors on $r_0(L)$, this does not significantly affect our results. Finally, the TF constraints also depend on Ω_0 (see equation 5). This effect has been taken into account in the middle right panel of Fig. 9 by rescaling $M/\bar{L}_{\rm c}$ and M accordingly so that we can plot the curves for different Ω_0 in the same figure.

Fig. 9 presents results for the best-fitting models with $\Omega_0 = 0.2$, 0.3, 0.4, 0.5 and 1.0. Models with $\Omega_0 \lesssim 0.3$ predict values of $r_0(L)$ that are too large, while models with $\Omega_0 \gtrsim 0.3$ predict too high values of $M/\bar{L}_{\rm c}$ to match the observed TF constraints. Apparently, *the technique used here is extremely effective in breaking the degeneracy between Ω_0 and σ_8* that is present in current measurements of cosmic shear and/or the abundance of rich galaxy clusters. Remarkably, the best results are obtained for Ω_0 close to the concordance value of $\Omega_0 = 0.3$, in good agreement with the constraints obtained from high redshift supernova Ia searches (e.g. Riess et al. 1998; Perlmutter et al. 1999) and from observations of the temperature anisotropies in the cosmic microwave background (e.g. Sievers et al. 2002).

For an Einstein–de Sitter cosmology, we find mass-to-light ratios that are more than an order of magnitude too high to match the TF constraints. This is in good agreement with previous studies based on a variety of different methods (e.g. White & Frenk 1991; Cole 1991; Kauffmann et al. 1993; Steinmetz & Navarro 1999; Elizondo et al. 1999; van den Bosch 2000).

6.2 The normalization of the power spectrum

In the previous section we have shown that models with $\Omega_0 = 0.3$ yield the best results, once σ_8 is kept normalized to the constraints obtained by Hoekstra et al. (2002). For the ΛCDM concordance model this implies $\sigma_8 = 0.86$. This normalization is consistent with constraints from the observed abundance of rich clusters of galaxies (e.g. White, Efstathiou & Frenk 1993; Eke, Cole & Frenk 1996; Bahcall & Fan 1998; Viana & Liddle 1996; Viana & Liddle 1999; Pierpaoli, Scott & White 2001) and from weak gravitational lensing studies (van Waerbeke et al. 2002; Bacon et al. 2002; Refregier, Rhodes & Groth 2002). However, a number of recent studies have suggested a somewhat lower normalization, of the order of $\sigma_8 = 0.7$–0.8 (e.g. Carlberg et al. 1997; Viana, Nichol & Liddle 2002; Seljak 2002a; Reiprich & Böhringer 2002). We therefore investigate the impact of such small changes in σ_8, while keeping the value of Ω_0 fixed at 0.3.

Changes in σ_8 mainly affects the clustering strength, which is proportional to $b^2\sigma_8^2$. The bias $b(M)$ increases with decreasing $\sigma(M)$ (Mo & White 1996), and since $\sigma(M) \propto \sigma_8$, lowering the value of σ_8 causes haloes of given mass to be more strongly biased. However, since on galactic scales the increase of b with $1/\sigma(M)$ is less rapid than linear, the clustering strength decreases when σ_8 is lowered. The upper panels of Fig. 10 compare our fiducial model M1 ($\sigma_8 = 0.9$) with models M7 ($\sigma_8 = 0.8$) and M8 ($\sigma_8 = 0.7$). Indeed, lower values of σ_8 result in smaller correlation lengths. In fact, for $\sigma_8 = 0.8$ the model yields an excellent fit to the observed $r_0(L)$. In addition, from the values of $\chi^2(\Phi)$ it is clear that these modest changes of σ_8 do not significantly influence the quality of the fit to the LF. However, the M/L ratios on the mass scale probed by the TF relation become slightly higher, therewith only worsening the problem of reproducing the correct TF zero-point. Thus, lowering σ_8 by about 10 per cent with respect to the concordance value brings the luminosity dependence of the galaxy clustering strengths in excellent agreement with observations, but an alternative or additional modification is required to bring the mass-to-light ratios in agreement with the TF zero-point.

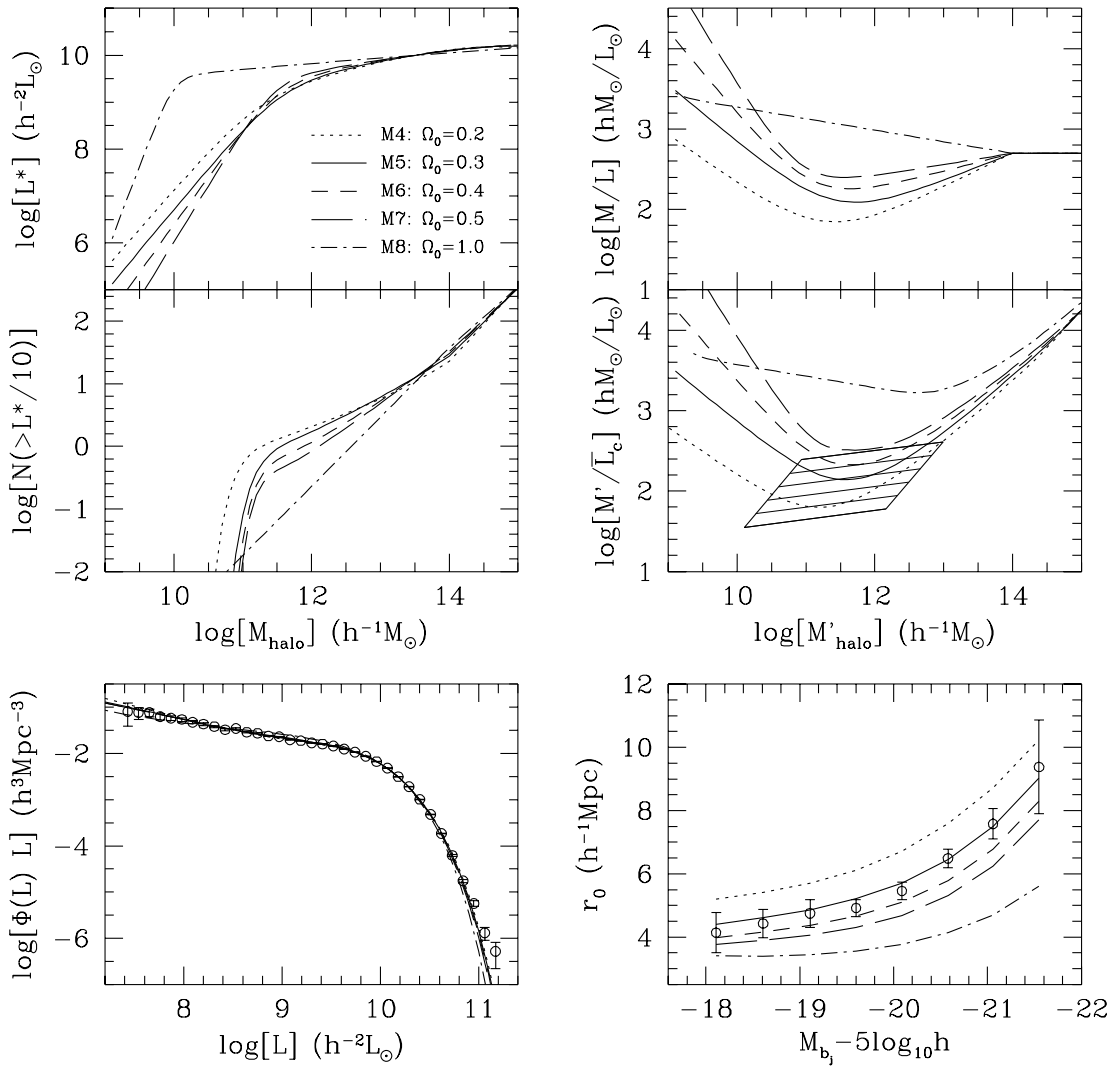

Figure 9. Same as Fig. 4 except that here we compare results for a number of ΛCDM models with different values for Ω_0 as indicated. All models have $\Omega_\Lambda = 1.0 - \Omega_0$, normalization $\sigma_8\Omega_0^{0.52} = 0.46$ (Hoekstra et al. 2002), and shape parameter $\Gamma = \Omega_0\, h$ with $h = 0.7$ (see Table 2). Note that the middle panel on the right plots $\log[M'/\bar{L}_c]$ rather than $\log[M/\bar{L}_c]$, and that these mass-to-light ratios are plotted as function of $M' = M(\Omega_0/0.3)^{b_{TF}/6}$. This takes care of the fact that the TF constraints depend on Ω_0 (see equation 5) and allows all models to be plotted in the same figure. Note also how models with $\Omega_0 > 0.35$ yield mass-to-light ratios that are too high, while models with $\Omega_0 < 0.25$ result in correlation lengths that are too large.

6.3 Tilted CDM models

So far we have only considered models with a Harrison–Zel'dovich power spectrum ($n = 1$). However, inflationary models allow small deviations of n from unity, and we therefore investigate the effect of small modifications of n.

The middle panels of Fig. 10 plot the results for models M9 ($n = 0.8$) and M10 ($n = 1.2$). In both models we keep the normalization of the power spectrum fixed at $\sigma_8 = 0.9$ and we adopt the cosmological parameters of the concordance model. Lowering n has the effect of suppressing the linear power spectrum on small scales, and so one might hope to reduce the number density of galactic haloes. We find this effect to be quite small, and so the mass-to-light ratios required to match the luminosity function are quite similar to those obtained for the concordance model with $n = 1$. The biggest effect of changing n is to change the correlation length of the mass, for example, the mass correlation length is about $5.1\,h^{-1}$ Mpc for $n = 0.8$, and about $4.7\,h^{-1}$ Mpc for $n = 1.2$. Since the bias factor for galaxies increases with decreasing n (because of the decrease in σ (M) on galaxy scales), the predicted correlation lengths for galaxies increases with decreasing n, as shown clearly in the middle right panel. Thus, an increase of the power index n has a similar effect as lowering σ_8; it brings the correlation lengths in better agreement with the data, while slightly increasing the mass-to-light ratios on the scale of galaxies.

6.4 Warm dark matter

In recent years there have been various claims that the CDM paradigm is in conflict with observations on small scales. First, CDM predicts too many low-mass haloes which leads to problems with the abundance of satellite galaxies around a typical Milky Way sized galaxy (e.g. Moore et al. 1999; Klypin et al. 1999; but see Stoehr et al. 2002) and to problems with the formation of disc galaxies (White & Navarro 1993; Navarro & Steinmetz 1999, 2000; Mo & Mao 2000; van den Bosch, Burkert & Swaters 2001). Secondly, CDM models predict dark matter haloes with steeply cusped density distributions, inconsistent with the observed rotation curves of some

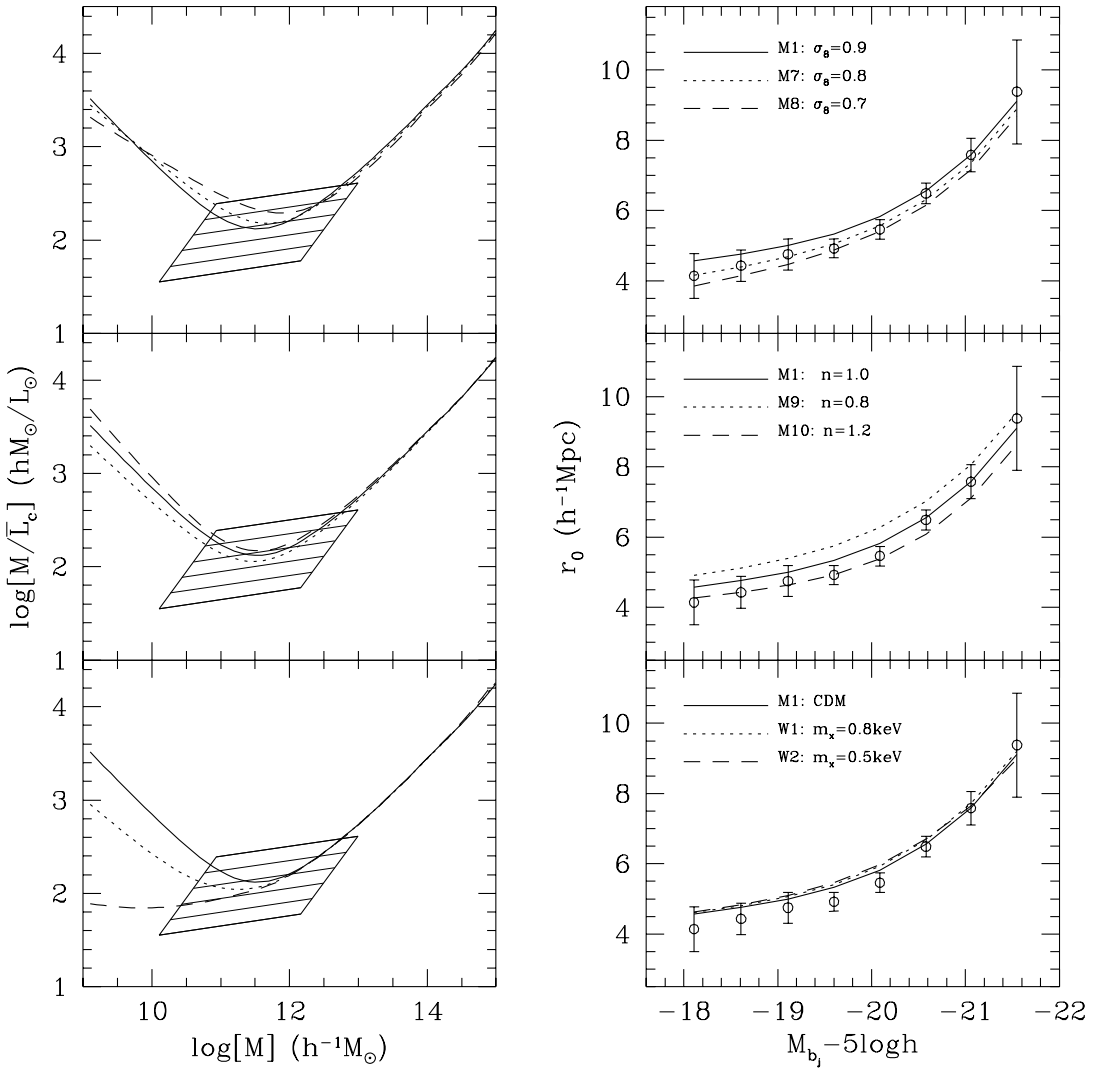

Figure 10. Same as Fig. 5 except that here we compare models in which we vary σ_8 (upper panels), the slope of the initial power spectrum n (middle panels), and the nature of the dark matter (lower panels) with respect to the fiducial model. All other cosmological parameters are kept the same as for the ΛCDM concordance cosmology.

dwarf and low surface brightness galaxies (e.g. Blais-Ouellette, Amram & Carignan 2001; de Blok et al. 2001; but see van den Bosch & Swaters 2001).

In order to (partially) alleviate these problems, warm dark matter (WDM) has been suggested as an alternative dark matter candidate (e.g. Sommer-Larsen & Dolgov 2001; Colín, Avila-Reese & Valenzuela 2000; Bode, Ostriker & Turok 2001). In WDM models the dark matter particles have a non-negligible initial velocity, which causes the damping of small-scale fluctuations due to free-streaming. Consequently the power-spectrum of WDM is modified with respect to that of CDM, and can be expressed in terms of the CDM power spectrum $P_{\rm CDM}(k)$ according to

$$P_{\rm WDM}(k) = T^2_{\rm WDM}(k) P_{\rm CDM}(k) \tag{47}$$

where the WDM transfer function is approximated by

$$T_{\rm WDM}(k) = \exp\left[-\frac{kR_{f,\rm WDM}}{2} - \frac{(kR_{f,\rm WDM})^2}{2}\right] \tag{48}$$

(Bardeen et al. 1986; Sommer-Larsen & Dolgov 2001). The comoving free-streaming scale $R_{f,\rm WDM}$ is related to a free-streaming mass $M_{f,\rm WDM}$ according to

$$M_{f,\rm WDM} = 3.7 \times 10^{14}\, h^{-1}\,{\rm M}_\odot\, \Omega_{\rm WDM} \left(\frac{R_{f,\rm WDM}}{h^{-1}\,{\rm Mpc}}\right)^3 \tag{49}$$

which in turn is related to the mass m_X of the WDM particles as

$$m_X = 2.4\, h^{5/4} \Omega^{1/2}_{\rm WDM} \left(\frac{M_{f,\rm WDM}}{10^{11}\, h^{-1}\,{\rm M}_\odot}\right)^{-1/4} {\rm keV}. \tag{50}$$

The lower two panels of Fig. 10 compare the results for our fiducial CDM model M1 with two WDM models, W1 and W2, that differ only in the mass of the WDM particles (see Table 2). Except for the properties of the dark matter, these models have the same cosmological parameters as the ΛCDM concordance model. Decreasing m_X causes a decrease in the abundance of small-mass haloes. Consequently, in order to preserve the abundance of (faint) galaxies, each (low-mass) halo needs to harbour more (or brighter) galaxies. This causes a decrease in the mass-to-light ratios. Furthermore, WDM haloes are expected to be somewhat less concentrated than their CDM counterparts (e.g. Bode et al. 2000), favouring lower values of $V_{\rm max}/V_{\rm vir}$. Both of these two effects bring the model in better

agreement with the TF constraint. On the other hand, the change from CDM to WDM does not significantly change the fit to the luminosity function and correlation lengths. It thus seems that WDM models with $m_X \lesssim 0.8$ are consistent with all data considered here. However, such low WDM particle masses may be hard to reconcile with the observed opacity distribution of the Lyα forest (Narayanan et al. 2000), with the phase-space densities of dwarf galaxies (Dalcanton & Hogan 2001), and with reionization constraints (Barkana, Haiman & Ostriker 2001). It thus remains to be seen to what extent WDM may be considered a successful alternative for the CDM paradigm.

7 COMPARISON WITH SEMI-ANALYTICAL MODELS FOR GALAXY FORMATION

The problem of simultaneously reproducing the galaxy LF and the TF zero-point has been noticed before in studies based on semi-analytical models for the formation of galaxies. Initially these studies focused on Einstein–de Sitter cosmologies, where the discrepancy was found to be very large (e.g. Kauffmann et al. 1993; Cole et al. 1994). This is in excellent agreement with our results, which indicate that cosmologies with $\Omega_0 = 1$ imply mass-to-light ratios that are more than an order of magnitude too large. Better results were obtained for cosmologies with lower values of Ω_0, but the overall agreement remained unsatisfactory (Heyl et al. 1995).

Further improvement was achieved by including dust obscuration in the modelling (Somerville & Primack 1999; Cole et al. 2000; Benson et al. 2000). As long as $V_{\rm max}/V_{\rm vir} = 1$ was adopted, these models found good agreement with the TF relation. However, using the more realistic values in accord with the NFW profiles of CDM haloes, the semi-analytical models predict too high rotation velocities at given luminosity. Similar results were obtained by studies that do not attempt to simultaneously reproduce the galaxy LF, but normalize the mass-to-light ratios of galaxy-sized haloes by adopting baryon fractions motivated by nucleosynthesis constraints (Steinmetz & Navarro 1999; Mo & Mao 2000; Navarro & Steinmetz 2000; van den Bosch 2000). Once again, our conclusions are in excellent agreement with these results.

In general, the semi-analytical models use the extended Press–Schechter formalism (Bond et al. 1991; Bower 1991; Kauffmann & White 1993; Lacey & Cole 1993; Somerville & Kolatt 1999) to compute Monte-Carlo realizations of the halo merger histories. Since this method yields no information about the spatial distribution of dark matter haloes, the clustering properties of galaxies can not be addressed. Various studies have therefore applied the semi-analytical models directly to dark matter haloes grown in cosmological simulations (Kauffmann et al. 1997, 1999; Diaferio et al. 1999; Benson et al. 2000, 2001; Springel et al. 2001; Mathis et al. 2002) and computed correlation functions of the model galaxies.

Benson et al. (2000) and Kauffmann et al. (1999) presented the mass-to-light ratios as function of virial mass for their models, which can be directly compared with the $\langle M/L\rangle(M)$ obtained from our conditional LF. Benson et al. (2000) find a clear minimum of $\sim 125\,h\,{\rm M}/{\rm L}_\odot$ at $M \approx 10^{12}\,h^{-1}\,{\rm M}_\odot$, while for $M \gtrsim 10^{14}\,h^{-1}\,{\rm M}_\odot$ their mass-to-light ratios converge to a value of $\sim 450\,h\,{\rm M}/{\rm L}_\odot$. The agreement with our fiducial model (see upper right panel of Fig. 4) is impressive, suggesting that their semi-analytical models result in a conditional LF not too different from the one derived here using a completely different approach. This is further supported by the fact that their models yield a luminosity dependence of the correlation length that is in reasonable agreement with our fiducial model.

This suggests that the technique introduced here, in addition to constraining cosmological parameters, can be used to place constraints on galaxy formation. For example, Kauffmann et al. (1999) showed that different treatments of star formation and feedback have a strong influence both on the slope and the amplitude of the two-point correlation function of galaxies. Benson et al. (2000), on the other hand, concluded that the predictions for the correlation function are robust to changes in the semi-analytical model parameters as long as the models match the bright end of the luminosity function. Our results, however, clearly indicate that different models, which fit the LF equally well, can have quite different clustering properties. For example, models M1A to M1F all match the LF roughly equally well (with the possible exception of M1B) but yield correlation lengths that differ quite strongly. This suggests that, as concluded by Kauffmann et al. (1999), the physics of galaxy formation (which set the conditional LF) has a strong effect on the clustering properties of galaxies.

The above discussion clearly indicates the potential strength of the technique introduced here. Note that our conclusions are independent of the uncertainties present in current theories of galaxy formation. In particular, no uncertain assumptions have to be made regarding the efficiencies of star formation and feedback, or regarding the effects of merging and dust obscuration. This makes the results presented here more robust. An additional advantage is the computational costs; only a few minutes are required to find the best-fitting parameters of the conditional LF for a specific cosmological model. Thus, our approach can be used to probe a large number of cosmological models in a relatively short time. On the other hand, the approach explored here has its limitations. It only yields a parametrized form of the conditional LF, and it is unclear if the best-fitting $\Phi(L\,|\,M)$ can be understood in terms of the physical processes governing galaxy formation. This may be most easily addressed with semi-analytical models, and as such the two approaches are complementary.

8 THE DISTRIBUTION OF LIGHT IN THE LOCAL UNIVERSE

The conditional luminosity function $\Phi(L\,|\,M)$ that we have attempted to constrain in this paper is a powerful tool in linking the distribution of galaxies to that of the dark matter. As an illustration, we use the $\Phi(L\,|\,M)$ of our fiducial model to present some statistical properties of the distribution of (blue) light (of galaxies) in the local Universe (i.e. at $z \simeq 0$). Note that these distributions only give an approximate description of the true distribution of light. After all, they correspond to our fiducial model, which is not perfectly consistent with all data. The description given here therefore only serves as an illustration of the statistical distributions that can be obtained once the conditional LF is known more accurately.

First we use $\Phi(L\,|\,M)$ to define the joint probability distribution

$$P(L,M)\,{\rm d}L{\rm d}M = \frac{1}{\bar{\rho}_L} n(M)\Phi(L\,|\,M)L\,{\rm d}L\,{\rm d}M \qquad (51)$$

which gives the probability that a b_j-band photon that is produced in the local Universe originates from a galaxy with luminosity in the range $L \pm {\rm d}L/2$ that resides in a halo with virial mass in the range $M \pm {\rm d}M/2$. Here $\bar{\rho}_L$ is the average luminosity density, given by

$$\begin{aligned}\bar{\rho}_L &= \int_0^\infty {\rm d}L\, L \int_0^\infty {\rm d}M\, n(M)\Phi(L\,|\,M) \\ &= \int_0^\infty \Phi(L)L\,{\rm d}L. \end{aligned} \qquad (52)$$

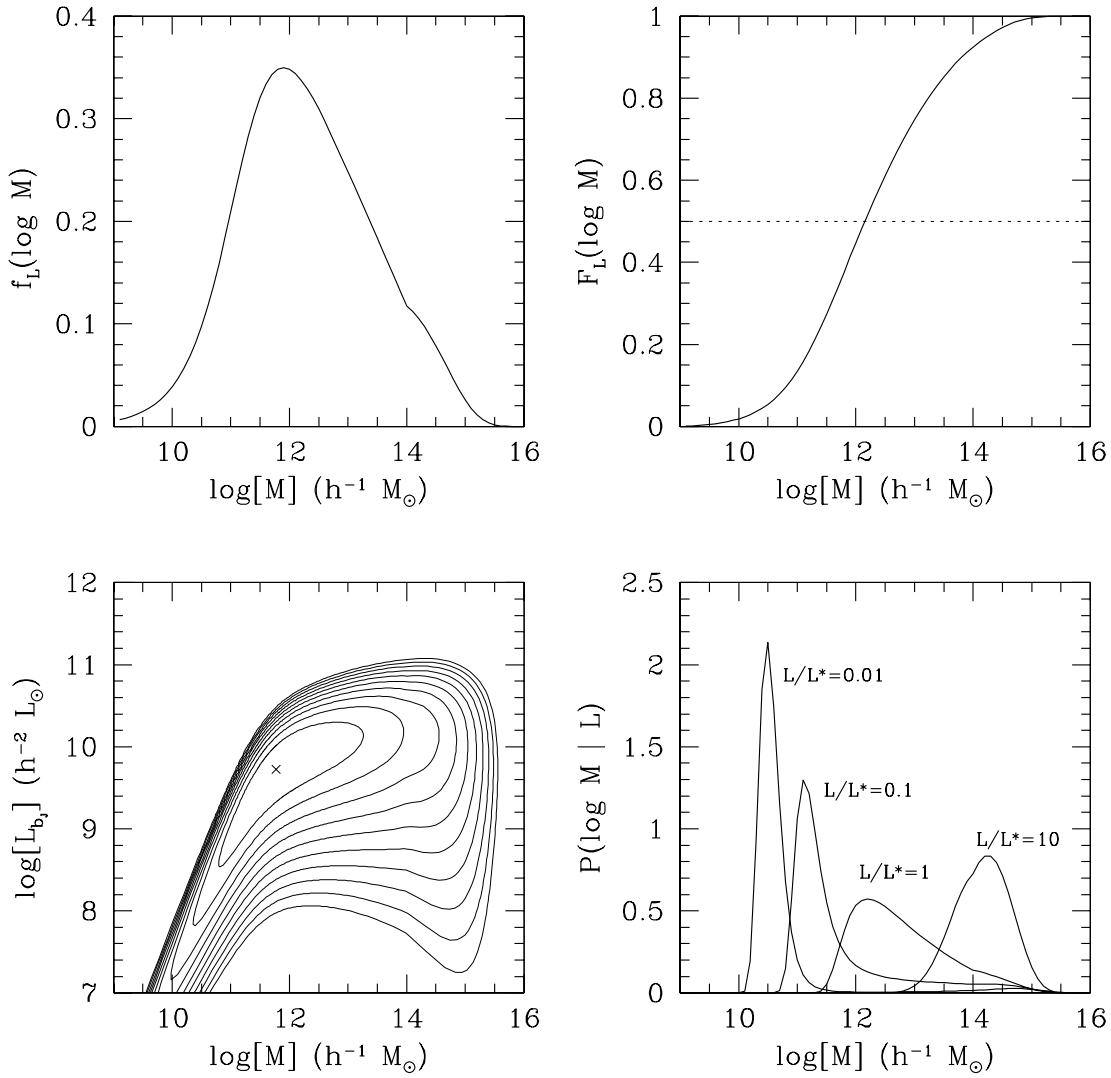

Figure 11. Statistics regarding the distribution of blue light at $z = 0$. The upper left panel plots the fraction of blue light emitted by galaxies inside haloes with virial masses in the range M, $M + \mathrm{d}M$. The corresponding cumulative distribution is shown in the upper right panel, indicating that ∼50 per cent of all blue light is produced inside haloes with $M < 2 \times 10^{12}\,h^{-1}\,\mathrm{M}_\odot$. The contour plot in the lower left panel corresponds to the joint probability distribution $P(L, M)$ (equation 51). The cross marks the maximum of $P(L, M)$, and the nth contour level is at 2^{-n} times the maximum. Note that galaxies with $L \simeq 10^{10}\,h^{-2}\,\mathrm{L}_\odot$ living inside haloes with $M \simeq 1 \times 10^{12}\,h^{-1}\,\mathrm{M}_\odot$ are the most efficient producers of blue light in the local Universe. Finally, the bottom right panel plots the conditional probability distributions $P(M \mid L)$ (equation 54) for four different luminosities as indicated.

The contours in the lower left panel of Fig. 11 show the joint probability distribution $P(L, M)$ for our fiducial model M1. As can be seen, the joint probability distribution peaks at around $L \simeq L^*$ and $M \simeq 1 \times 10^{12}\,h^{-1}\,\mathrm{M}_\odot$, i.e. these systems are the most efficient producers of blue light in the local Universe. Integrating $P(L, M)$ over all luminosities yields the fraction of all light, $f_L(M)\,\mathrm{d}M$, produced by galaxies inside haloes with virial masses in the range $M \pm \mathrm{d}M/2$:

$$f_L(M) = \int_0^\infty P(L, M)\,\mathrm{d}L = \frac{1}{\bar{\rho}_L} n(M)\langle L\rangle(M). \tag{53}$$

The upper left panel of Fig. 11 plots f_L as function of halo mass again for the conditional LF of our fiducial model. Note that haloes with $M \sim 10^{12}\,h^{-1}\,\mathrm{M}_\odot$ are the most productive in 'producing' light. This is not surprising, given that $\langle M/L\rangle(M)$ reaches a minimum at around this mass scale. This is also consistent with generic models of galaxy formation, which predict that haloes more massive than $10^{12}\,h^{-1}\,\mathrm{M}_\odot$ are inefficient in cooling their baryonic gas, while less massive haloes are inefficient in producing stars because of heating from supernova feedback (e.g. Larson 1974; White & Rees 1978; Dekel & Silk 1986).

The upper right panel of Fig. 11 plots the cumulative distribution $F(<M) = \int_0^M f_L(M)\,\mathrm{d}M$, which gives the fraction of all light produced in haloes less massive than M. In our fiducial model, about 50 per cent of all light is produced inside haloes with $M \lesssim 2 \times 10^{12}\,h^{-1}\,\mathrm{M}_\odot$. Since this is roughly the mass scale where one changes from isolated haloes around galaxies to haloes that harbour groups and clusters of galaxies, this indicates that isolated galaxies produce roughly the same amount of light as galaxies residing in clusters and groups. Note also that the distribution of $f_L(M)$ is quite narrow. Galaxies in haloes with $M \gtrsim 2 \times 10^{14}\,h^{-1}\,\mathrm{M}_\odot$ and $M \lesssim 5 \times 10^{10}\,h^{-1}\,\mathrm{M}_\odot$ each are responsible for only about 5 per cent of the total blue light in the local Universe.

Finally, we use the conditional LF to compute the conditional probability distribution $P(M \mid L)\,\mathrm{d}M$ that a galaxy of luminosity L

lives inside a halo with virial mass in the range $M \pm \mathrm{d}M/2$. Using Bayes' theorem,

$$P(M \mid L)\,\mathrm{d}M = \frac{\Phi(L \mid M)}{\Phi(L)} n(M)\,\mathrm{d}M. \tag{54}$$

The lower right panel of Fig. 11 plots this probability distribution for four different luminosities: $L = L^*/100$, $L = L^*/10$, $L = L^*$, $L = 10L^*$. Whereas $10L^*$ galaxies are typically found in haloes with $10^{13}h^{-1} \lesssim M \lesssim 10^{15}\,h^{-1}\,\mathrm{M}_\odot$, galaxies with $L = L^*/100 \sim 10^8\,h^{-2}\,\mathrm{L}_\odot$ typically reside in haloes of $M \simeq 5 \times 10^{10}\,h^{-1}\,\mathrm{M}_\odot$. Only a very small fraction of these galaxies ($\lesssim$5 per cent) are found as a member of a larger group or cluster of galaxies. It should be pointed out, however, that our model predictions for $P(M \mid L)$ are quite uncertain for galaxies with $L \lesssim L^*/10$. This is a result of the fact that constraints on $r_0(L)$ only exist for galaxies with $L > L^*/5$, even though data on the luminosity function extend down to much fainter luminosities. If, for example, for $L < L^*/5$ the correlation lengths increase with decreasing luminosity (i.e. opposite to the trend for the brighter galaxies), we would obtain conditional luminosity functions with many more faint galaxies in massive haloes than in the current prediction. Clearly, observational data on the correlation functions of faint galaxies are needed in order better to constrain their $P(M \mid L)$.

9 CONCLUSIONS

We have presented a novel technique to link the distribution of galaxies to that of dark matter haloes. This technique extends upon earlier modelling of halo occupation number distributions by labelling the galaxies with luminosities. In particular, we have introduced the conditional luminosity function $\Phi(L \mid M)\,\mathrm{d}L$, which gives the average number of galaxies with luminosities in the range $L \pm \mathrm{d}L/2$ that reside in a halo of mass M. Starting from the number density of CDM haloes, $n(M)\,\mathrm{d}M$, we sought the $\Phi(L \mid M)$ that reproduces the 2dFGRS b_j-band luminosity function $\Phi(L)\,\mathrm{d}L$. Since there are many different $\Phi(L \mid M)$ that are consistent with both $n(M)$ and $\Phi(L)$, we used the luminosity dependence of the galaxy correlation lengths obtained from the 2dFGRS as additional constraints. This allows the recovery of a unique best-fitting $\Phi(L \mid M)$. To assess the viability of the conditional LF thus found, we used $\Phi(L \mid M)$ to compute the average mass-to-light ratios of dark matter haloes as function of mass, which we compared with constraints obtained from the (zero-point of) the TF relation.

For the ΛCDM concordance cosmology ($\Omega_0 = 0.3$, $\Omega_\Lambda = 0.7$, $h = 0.7$, $\sigma_8 = 0.9$), we are able to accurately reproduce the observed LF. In addition, adopting a simple model for the distribution of galaxies inside dark matter haloes, we obtain galaxy–galaxy correlation functions as function of luminosity that are in agreement with the data of Norberg et al. (2001). However, the values of $\langle M/L \rangle$ we obtained are slightly too high to match that implied by the TF relation.

We have shown that the concordance model can be made consistent with the data if either the 2dFGRS is only ~70 per cent complete (which is very unlikely), or if ~30 per cent of all dark matter haloes have failed to form observable galaxies (they only contain 'dark' galaxies). Although feedback and an ionizing background can explain the presence of such dark galaxies in low-mass haloes, there is currently no clear mechanism that can prevent star formation in more massive haloes, rendering this option unlikely as well (but see Verde et al. 2002).

The mass-to-light ratios of the concordance model can also be brought into agreement with the TF constraints if H_0 is lowered to ~55 km s^{-1} Mpc^{-1}. Although this value is only marginally consistent with the recently advocated value of $H_0 = 72 \pm 8$ km s^{-1} Mpc^{-1} (68 per cent confidence) of the *HST* Key Program (Freedman et al. 2001), such low value is in agreement with recent time-delay measurements in gravitational lens systems (Kochanek 2002; but see also Hjorth et al. 2002). Alternatively, $\langle M/L \rangle$ may be lowered by adopting warm, rather than cold dark matter. In WDM cosmologies the abundance of low-mass haloes is suppressed, resulting in lower mass-to-light ratios; WDM haloes are also expected to be less concentrated than CDM haloes and so the mass-to-light ratios implied by the observed TF relation is also higher. Both of these effects lead to better agreement between the model predictions and the TF constraints. In order to have a significant effect, we find that the WDM particles must have a mass of the order of $m_X \lesssim 0.8$ keV, which is already the lower limit set by a number of other observational constraints (Narayanan et al. 2000; Dalcanton & Hogan 2001; Barkana et al. 2001).

In addition to these modifications of the concordance cosmology, we have also investigated cosmologies with different matter densities. We have shown that the technique presented here allows one to break the degeneracy between Ω_0 and σ_8 inherent in the cosmological constraints obtained from cosmic shear and/or cluster abundance measurements. The best results are obtained for $\Omega_0 \simeq 0.3$, in good agreement with the high redshift supernova results (e.g. Riess et al. 1998; Perlmutter et al. 1999): for $\Omega_0 \gtrsim 0.4$ the mass-to-light ratios of dark matter haloes are too high to match the TF zero-point, while cosmologies with $\Omega_0 \lesssim 0.2$ yield correlation lengths that are too large.

In summary, the modelling of the conditional LF presented here strongly favours a cosmology with $\Omega_0 \simeq 0.3$. However, in order to bring the models into agreement with the observed zero-point of the TF relation, either h is lowered by 15 to 20 per cent with respect to the concordance values of 0.7, dark matter is warm rather than cold, or a large fraction of haloes host no luminous galaxies.

Once a satisfactory model for the conditional LF is found, it can be used to extract useful statistical information about the distribution of light in the Universe. As an example, we have computed the fractional contribution to the total luminosity density by galaxies with luminosity L that live in haloes of mass M. In particular, we have shown that 50 per cent of all the blue light is produced in haloes with $M \lesssim 2 \times 10^{12}\,h^{-1}\,\mathrm{M}_\odot$. In addition, the conditional LF can be used to compute the probability $P(M \mid L)\,\mathrm{d}M$ that a galaxy with luminosity L lives in a halo with mass in the range $M \pm \mathrm{d}M/2$. These probability distributions may prove useful for a statistical interpretation of the mass-to-light ratios inferred from, for example, galaxy kinematics or gravitational lensing.

The technique presented here can easily be extended to compute higher-order correlation functions, as well as pair-wise peculiar velocity dispersions, all as function of galaxy luminosity. In the near future several large redshift surveys of galaxies will become available, such as the SDSS and the completed 2dFGRS at $z \simeq 0$ and DEEP and VIRMOS at $z \simeq 1$. These will allow far more stringent constraints to be placed on cosmological parameters, especially when combined with the complementary constraints from weak-lensing and cluster abundances. In addition, once luminosity functions and correlation lengths are available in different photometric passbands and for different morphological classes, the technique presented here can easily be extended to model simultaneously the distribution of galaxies as function of colour and/or morphological type. This will not only help to constrain cosmological parameters, but also to provide important insights into the complicated processes associated with galaxy formation.

ACKNOWLEDGMENTS

We are grateful to Shaun Cole and Peder Norberg for providing the 2dFGRS luminosity functions in several cosmological models used in this paper. We thank both Simon White and the referee for insightful comments and for careful reading of the paper, and Andreas Berlind, Peder Norberg, Rachel Somerville, David Weinberg and Saleem Zaroubi for useful discussions. XY thanks the MPG-CAS student exchange program for financial support.

REFERENCES

Bacon D., Massey R., Refregier A., Ellis R., 2002, preprint (astro-ph/0203134)
Bahcall N. A., Fan X., 1998, ApJ, 504, 1
Bardeen J. M., Bond J. R., Kaiser N., Szalay A., 1986, ApJ, 304, 15
Barkana R., Haiman Z., Ostriker J. P., 2001, ApJ, 558, 482
Barnes J. E., White S. D. M., 1984, MNRAS, 211, 753
Baugh C. M., 1996, MNRAS, 282, 1413
Beijersbergen M., Hoekstra H., van Dokkum P. G., van der Hulst T., 2002, MNRAS, 329, 385
Benoist C., Maurogordato S., Da Costa L. N., Cappi A., Schaeffer R., 1996, ApJ, 472, 452
Benson A. J., Cole S., Frenk C. S., Baugh C. M., Lacey C. G., 2000, MNRAS, 311, 793
Benson A. J., Frenk C. S., Baugh C. M., Cole S., Lacey C. G., 2001, MNRAS, 327, 1041
Benson A. J., Lacey C. G., Baugh C. M., Cole S., Frenk C. S., 2002, MNRAS, 333, 156
Berlind A. A., Weinberg D. H., 2002, ApJ, 575, 587
Blair M., Gilmore G., 1982, PASP, 94, 741
Blais-Ouellette S., Amram P., Carignan C., 2001, AJ, 121, 1952
Blanton M. R. et al., 2001, AJ, 121, 2358
Blumenthal G. R., Faber S. M., Flores R., Primack J. R., 1986, ApJ, 301, 27
Bode P., Ostriker J. P., Turok N., 2001, ApJ, 556, 93
Bond J. R., Cole S., Efstathiou G., Kaiser N., 1991, ApJ, 379, 440
Börner G., Mo H. J., Zhou Y. Y., 1989, A&A, 221, 191
Bower R., 1991, MNRAS, 248, 332
Bullock J. S., Dekel A., Primack J. R., Somerville R. S., 2001a, ApJ, 550, 21
Bullock J. S., Kolatt T. S., Sigad Y., Somerville R. S., Klypin A. A., Primack J. R., Dekel A., 2001b, MNRAS, 321, 559
Bullock J. S., Wechsler R. H., Somerville R. S., 2002, MNRAS, 329, 246
Carlberg R. G., Morris S. L., Yee H. K. C., Ellingson E., 1997, ApJ, 479, L19
Cole S., 1991, ApJ, 367, 45
Cole S., Kaiser N., 1989, MNRAS, 237, 1127
Cole S., Aragon-Salamanca A., Frenk C. S., Navarro J. F., Zepf S. E., 1994, MNRAS, 271, 781
Cole S., Lacey C. G., Baugh C. M., Frenk C. S., 2000, MNRAS, 319, 168
Colín P., Avila-Reese V., Valenzuela O., 2000, ApJ, 542, 622
Dalcanton J. J., Hogan C. J., 2001, ApJ, 561, 35
Davis M., Peebles P. J. E., 1983, ApJ, 267, 465
de Bernardis P. et al., 2002, ApJ, 564, 559
de Blok W. J. G., McGaugh S. S., Bosma A., Rubin V. C., 2001, ApJ, 552, L23
de Jong R. S., 1996, A&A, 313, 377
Dekel A., Silk J., 1986, ApJ, 303, 39
Diaferio A., Kauffmann G., Colberg J. M., White S. D. W., 1999, MNRAS, 307, 537
Efstathiou G., Ellis R. S., Peterson B. S., 1988a, MNRAS, 232, 431
Eke V. R., Cole S., Frenk C. S., 1996, MNRAS, 282, 263
Elizondo D., Yepes G., Kates R., Müller V., Klypin A., 1999, ApJ, 515, 525
Fardal M. A., Katz N., Gardner J. P., Hernquist L., Weinberg D. H., Dav'e R., 2001, ApJ, 562, 605
Flores R., Primack J. R., Blumenthal G. R., Faber S. M., 1993, ApJ, 412, 443
Folkes S. et al., 1999, MNRAS, 308, 459
Freedman W. L. et al., 2001, ApJ, 553, 47
Fry J. N., 1996, ApJ, 461, L65
Fukugita M., Hogan C. J., Peebles P. J. E., 1998, ApJ, 503, 518
Gonzales A. H., Williams K. A., Bullock J. S., Kolatt T. S., Primack J. R., 2000, ApJ, 528 145
Governato F., Babul A., Quinn T., Tozzi P., Baugh C. M., Katz N., Lake G., 1999, MNRAS, 307, 949
Gross M. A. K., Somerville R. S., Primack J. R., Holtzman J., Klypin A. A., 1998, MNRAS, 301, 81
Guzik J., Seljak U., 2002, MNRAS, 335, 311
Guzzo L. et al., 2000, A&A, 355, 1
Hawkins E., Maddox S. J., Branchini E., Saunders W., 2001, MNRAS, 325, 589
Heyl J. S., Cole S., Frenk C. S., Navarro J. F., 1995, MNRAS, 274, 755
Hjorth J. et al., 2002, ApJ, 572, L11
Hoekstra H., Yee H., Gladders M., 2002, ApJ, 577, 595
Jain B., Bertschinger E., 1994, ApJ, 431, 495
Jenkins A., Frenk C. S., White S. D. M., Colberg J. M., Cole S., Evrard A. E., Couchman H. M. P., Yoshida N., 2001, MNRAS, 321, 372
Jimenez R., Heavens A. F., Hawkins M. R. S., Padoan P., 1997, MNRAS, 292, L5
Jimenez R., Verde L., Oh S. P., 2002, preprint (0201352)
Jing Y. P., 1998, ApJ, 503 L9
Jing Y. P., 2000, ApJ, 535, 30
Jing Y. P., Mo H. J., Börner G., 1998, ApJ, 494, 1
Jing Y. P., Börner G., Suto Y., 2002, ApJ, 564, 15
Kaiser N., 1984, ApJ, 284, L9
Kang X., Jing Y. P., Mo H. J., Börner G., 2002, MNRAS, 336, 892
Katz N., Weinberg D. H., Hernquist L., 1996, ApJS, 105, 19
Kauffmann G., White S. D. M., 1993, MNRAS, 261, 921
Kauffmann G., White S. D. M., Guiderdoni B., 1993, MNRAS, 264, 201
Kauffmann G., Nusser A., Steinmetz M., 1997, MNRAS, 286, 795
Kauffmann G., Colberg J. M., Diaferio A., White S. D. M., 1999, MNRAS, 303, 188
Kay S. T., Pearce F. R., Frenk C. S., Jenkins A., 2002, MNRAS, 330, 113
Klypin A. A., Gottlöber S., Kravtsov A. V., Khokhlov A. M., 1999, ApJ, 516, 530
Kochanek C. S., 2001, preprint (astro-ph/0108160)
Kochanek C. S., 2002, preprint (astro-ph/0204043)
Lacey C., Cole S., 1993, MNRAS, 262, 627
Larson R. B., 1974, MNRAS, 169, 229
Lemson G., Kauffmann G., 1999, MNRAS, 302, 111
Lin H., Kirschner R. P., Schectman S. A., Landy S. D., Oemler A., Tucker D. L., Schechter P. L., 1996, ApJ, 464, 60
Loveday J., Efstathiou G., Peterson B. A. Maddox S. J., 1992, ApJ, 400, L43
Loveday J., Maddox S. J., Efstathiou G., Peterson B. A., 1995, ApJ, 442, 457
Ma C. P., Fry J. N., 2000, ApJ, 543, 503
Marinoni C., Hudson M. J., 2002, ApJ, 569, 101
Marzke R. O., Huchra J. P., Geller M. J., 1994, ApJ, 428, 43
Mathis H., Lemson G., Springel V., Kauffmann G., White S. D. M., Eldar A., Dekel A., 2002, MNRAS, 333, 739
McClelland J., Silk J., 1977, ApJ, 217, 331
McKay T. A. et al., 2001, preprint (astro-ph/0108013)
McKay T. A. et al., 2002, ApJ, 571, L85
Melchiorri A. et al., 2000, ApJ, 536, L63
Mo H. J., Mao S., 2000, MNRAS, 318, 163
Mo H. J., White S. D. M., 2002, MNRAS, 336, 112
Mo H. J., White S. D. M., 1996, MNRAS, 282, 347
Mo H. J., Jing Y. P., White S. D. M., 1997, MNRAS, 284, 189
Mo H. J., Mao S., White S. D. M., 1998, MNRAS, 295, 319
Moore B., Ghigna S., Governato F., Lake G., Quinn T., Stadel J., Tozzi P., 1999, ApJ, 524, L19
Muriel H., Valotto C. A., Lambas D. G., 1998, ApJ, 506, 540
Narayanan V. K., Spergel D. N., Davé R., Ma C., 2000, ApJ, 543, L103
Navarro J. F., Steinmetz M., 1999, ApJ, 513, 555
Navarro J. F., Steinmetz M., 2000, ApJ, 538, 477

Navarro J. F., Frenk C. S., White S. D. M., 1997, ApJ, 490, 493
Newman J. A., Davis M., 2000, ApJ, 534, L11
Neyman J., Scott E. L., 1952, ApJ, 116, 144
Norberg P. et al., 2001, MNRAS, 328, 64
Norberg P. et al., 2002, MNRAS, 336, 907
Park C., Vogeley M. S., Geller M. J., Huchra J. P., 1994, ApJ, 431, 569
Peacock J. A., Dodds S. J., 1996, MNRAS, 280, L19
Peacock J. A., Smith R. E., 2000, MNRAS, 318, 1144
Pearce F. R., Thomas P. A., Couchman H. M. P., Edge A. C., 2000, MNRAS, 317, 1029
Perlmutter S. et al., 1999, ApJ, 517, 565
Pierpaoli E., Scott D., White M., 2001, MNRAS, 325, 77
Press W. H., Schechter P., 1974, ApJ, 187, 425
Press W. H., Teukolsky S. A., Vetterling W. T., Flannery B. P., 1992, Numerical Recipes. Cambridge, Cambridge Univ. Press
Refregier A., Rhodes J., Groth E. J., 2002, ApJ, 572, L131
Reiprich T. H., Böhringer H., 2002, ApJ, 567, 716
Riess A. G. et al., 1998, AJ, 116, 1009
Riess A. G. et al., 2001, ApJ, 560, 49
Saha A., Sandage A., Tammann G. A. Dolphin A. E., Christensen J., Panagia N., Macchetto F. D., 2001, ApJ, 562, 314
Schechter P., 1976, ApJ, 203, 297
Schlegel D. J., Finkbeiner D. P., Davis M., 1998, ApJ, 500, 525
Scoccimarro R., Sheth R. K., Hui L., Jain B., 2001, ApJ, 546, 20
Scranton R., 2002, MNRAS, 332, 697
Seljak U., 2000, MNRAS, 318, 203
Seljak U., 2002a, MNRAS, 337, 769
Seljak U., 2002b, MNRAS, 337, 774
Sheth R. K., Tormen G., 1999, MNRAS, 308, 119
Sheth R. K., Mo H. J., Tormen G., 2001, MNRAS, 323, 1
Sievers J. L. et al., 2002, preprint (astro-ph/0205387)
Shimasaku K., 1993, ApJ, 413, 59
Somerville R. S., Kolatt T. S., 1999, MNRAS, 305, 1
Somerville R. S., Primack J. R., 1999, MNRAS, 310, 1087
Sommer-Larsen J., Dolgov A., 2001, ApJ, 551, 608
Springel V., White S. D. M., Tormen G., Kauffmann G., 2001, MNRAS, 328, 726
Steinmetz M., Navarro J. F., 1999, ApJ, 513, 555
Stoehr F., White S. D. M., Tormen G., Springel V., 2002, MNRAS, 335, L84
Szapudi I., Branchini E., Frenk C. S., Maddox S., Saunders W., 2000, MNRAS, 318, L45
Tormen G., 1998, MNRAS, 297, 648
Trentham N., Hodgkin S., 2002, MNRAS, 333, 423
Tully R. B., Pierce M. J., 2000, ApJ, 533, 744
van den Bosch F. C., 2000, ApJ, 530, 177
van den Bosch F. C., 2001, MNRAS, 327, 1334
van den Bosch F. C., 2002, MNRAS, 332, 456
van den Bosch F. C., Swaters R. A., 2001, MNRAS, 325, 1017
van den Bosch F. C., Burkert A., Swaters R. A., 2001, MNRAS, 326, 1205
Verde L., Oh S. P., Jimenez R., 2002, MNRAS, 336, 541
Viana P. T. P., Liddle A. R., 1996, MNRAS, 281, 323
Viana P. T. P., Liddle A. R., 1999, MNRAS, 303, 535
Viana P. T. P., Nichol R. C., Liddle A. R., 2002, ApJ, 569, L75
van Waerbeke L., Mellier Y., Pello R., Pen U.-L., McCracken H. J., Jain B., 2002, A&A, 358, 30
White S. D. M., Frenk C., 1991, ApJ, 379, 52
White S. D. M., Rees M. J., 1978, MNRAS, 183, 341
White M., 2001, MNRAS, 321, 1
White S. D. M., Navarro J. F., 1993, MNRAS, 265, 271
White S. D. M., Efstathiou G., Frenk C. S., 1993, MNRAS, 262, 1023
Willmer C. N. A., Da Costa L. N., Pellegrini P. S., 1998, AJ, 115, 869
Yang X., Mo H. J., Kauffmann G., Chu Y., 2002, preprint (astro-ph/0205546)
Zehavi I. et al., 2002, ApJ, 571, 172
Zheng Z., Tinker J. L., Weinberg D. H., Berlind A. A., 2002, ApJ, 575, 617
Zucca E., 1997, A&A, 326, 477

This paper has been typeset from a TEX/LATEX file prepared by the author.